

1 | ["Projections of oceanic N<sub>2</sub>O emissions in the 21<sup>st</sup> century using the IPSL Earth System](#)  
2 | [Model"](#)

3 | J. Martinez-Rey<sup>1</sup>, L. Bopp<sup>2</sup>, M. Gehlen<sup>3</sup>, A. Tagliabue<sup>4</sup> and N. Gruber<sup>5</sup>.

4 |

5 | <sup>1</sup> Laboratoire des Sciences du Climat et de l'Environnement, IPSL, CEA/CNRS/UVSQ,  
6 | Bat. 712 - Orme des Merisiers, F-91191 CE Saclay, Gif-sur-Yvette, France.

7 | [jorge.martinez-rey@lsce.ipsl.fr](mailto:jorge.martinez-rey@lsce.ipsl.fr)

8 |

9 | <sup>2</sup> Laboratoire des Sciences du Climat et de l'Environnement, IPSL, CEA/CNRS/UVSQ,  
10 | Bat. 712 - Orme des Merisiers, F-91191 CE Saclay, Gif-sur-Yvette, France.

11 | [laurent.bopp@lsce.ipsl.fr](mailto:laurent.bopp@lsce.ipsl.fr)

12 |

13 | <sup>3</sup> Laboratoire des Sciences du Climat et de l'Environnement, IPSL, CEA/CNRS/UVSQ,  
14 | Bat. 712 - Orme des Merisiers, F-91191 CE Saclay, Gif-sur-Yvette, France.

15 | [marion.gehlen@lsce.ipsl.fr](mailto:marion.gehlen@lsce.ipsl.fr)

16 |

17 | <sup>4</sup> School of Environmental Sciences, University of Liverpool, 4 Brownlow Street,  
18 | Liverpool L69 3GP, UK.

19 | [a.tagliabue@liverpool.ac.uk](mailto:a.tagliabue@liverpool.ac.uk)

20 |

21 | <sup>5</sup> Environmental Physics, Institute of Biogeochemistry and Pollutant Dynamics, ETH,  
22 | CHN E31.2, Universitaetstrasse 16, 8092 Zürich, Switzerland.

23 | [nicolas.gruber@env.ethz.ch](mailto:nicolas.gruber@env.ethz.ch)

24 |

Jorge 4/1/15 10:32 AM

Deleted: 0

26 0. Abstract

27

28 The ocean is a substantial source of nitrous oxide (N<sub>2</sub>O) to the atmosphere, but little is  
29 known on how this flux might change in the future. Here, we investigate the potential  
30 evolution of marine N<sub>2</sub>O emissions in the 21<sup>st</sup> century in response to anthropogenic  
31 climate change using the global ocean biogeochemical model NEMO-PISCES. Assuming  
32 nitrification as the dominant N<sub>2</sub>O formation pathway, we implemented two different  
33 parameterizations of N<sub>2</sub>O production, which differ primarily at low oxygen (O<sub>2</sub>)  
34 conditions. When forced with output from a climate model simulation run under the  
35 business-as-usual high CO<sub>2</sub> concentration scenario (RCP8.5), our simulations suggest a  
36 decrease of 4 to 12 % in N<sub>2</sub>O emissions from 2005 to 2100, i.e., a reduction from 4.03 /  
37 3.71 to 3.54 / 3.56 TgN yr<sup>-1</sup> depending on the parameterization. The emissions decrease  
38 strongly in the western basins of the Pacific and Atlantic oceans, while they tend to  
39 increase above the Oxygen Minimum Zones (OMZs), i.e., in the Eastern Tropical Pacific  
40 and in the northern Indian Ocean. The reduction in N<sub>2</sub>O emissions is caused on the one  
41 hand by weakened nitrification as a consequence of reduced primary and export  
42 production, and on the other hand by stronger vertical stratification, which reduces the  
43 transport of N<sub>2</sub>O from the ocean interior to the ocean surface. The higher emissions over  
44 the OMZ are linked to an expansion of these zones under global warming, which leads to  
45 increased N<sub>2</sub>O production associated primarily with denitrification. While there are  
46 many uncertainties in the relative contribution and changes in the N<sub>2</sub>O production  
47 pathways, the increasing storage seems unequivocal and determines largely the decrease in  
48 N<sub>2</sub>O emissions in the future. From the perspective of a global climate system, the  
49 averaged feedback strength associated with the projected decrease in oceanic N<sub>2</sub>O  
50 emissions amounts to around -0.009 W m<sup>-2</sup>K<sup>-1</sup>, which is comparable to the potential  
51 increase from terrestrial N<sub>2</sub>O sources. However, the assesment for a compensation  
52 between the terrestrial and marine feedbacks calls for an improved representation of N<sub>2</sub>O  
53 production terms in fully coupled next generation of Earth System Models.

54

Jorge 4/1/15 6:12 PM

Deleted: w

Jorge 4/1/15 6:12 PM

Deleted: ,

57 1 Introduction

58

59 Nitrous oxide (N<sub>2</sub>O) is a gaseous compound responsible for two key feedback  
60 mechanisms within the Earth's climate. First, it acts as a long-lived and powerful  
61 greenhouse gas (Prather et al., 2012) ranking third in anthropogenic radiative forcing  
62 after carbon dioxide (CO<sub>2</sub>) and methane (CH<sub>4</sub>) (Myrhe et al., 2013). Secondly, the  
63 ozone (O<sub>3</sub>) layer depletion in the future might be driven mostly by N<sub>2</sub>O after the drastic  
64 reductions in CFCs emissions start to show their effect on stratospheric chlorine levels  
65 (Ravishankara et al., 2009). The atmospheric concentration of N<sub>2</sub>O is determined by the  
66 natural balance between sources from land and ocean and the destruction of N<sub>2</sub>O in the  
67 atmosphere largely by [photolysis](#) (Crutzen, 1970; Johnston, 1971). The natural sources  
68 from land and ocean amount to ~6.6 and 3.8 TgN yr<sup>-1</sup>, respectively (Ciais et al., 2013).  
69 Anthropogenic activities currently add an additional 6.7 TgN yr<sup>-1</sup> to the atmosphere,  
70 [which has](#) caused atmospheric N<sub>2</sub>O to increase by 18% since pre-industrial times (Ciais  
71 et al., 2013), reaching 325 ppb in the year 2012 (NOAA ESRL Global Monitoring  
72 Division, Boulder, Colorado, USA, <http://esrl.noaa.gov/gmd/>).

73 Using a compilation of 60,000 surface ocean observations of the partial pressure of N<sub>2</sub>O  
74 (pN<sub>2</sub>O), Nevison et al. (2004) computed a global ocean source of 4 TgN yr<sup>-1</sup>, with a  
75 large range of uncertainty from 1.2 to 6.8 TgN yr<sup>-1</sup>. Model derived estimates also differ  
76 widely, i.e., between 1.7 and 8 TgN yr<sup>-1</sup> (Nevison et al., 2003; Suntharalingam et al.,  
77 2000). These large uncertainties are a consequence of too few observations and of poorly  
78 known N<sub>2</sub>O formation mechanisms, reflecting a general lack of understanding of key  
79 elements of the oceanic nitrogen cycle (Gruber and Galloway, 2008; Zehr and Ward,  
80 2002), and of N<sub>2</sub>O in particular (e.g., Zamora et al., 2012, Bange et al., 2009 or Freing  
81 et al., 2012, among others). A limited number of interior ocean N<sub>2</sub>O observations were  
82 made available only recently (Bange et al., 2009), but they contain large temporal and  
83 spatial gaps. Information on the rates of many important processes remains insufficient,  
84 particularly in natural settings. There are only few studies from a limited number of  
85 specific regions such as the Arabian Sea, Central and North Pacific, [Black Sea](#), the  
86 Bedford Basin and the Scheldt estuary, which can be used to derive and test model  
87 parameterisations (Mantoura et al., 1993; Bange et al., 2000; Elkins et al., 1978; [Farias et](#)  
88 [al., 2007](#); [Frame and Casciotti, 2010](#); [Westley et al., 2006](#); Yoshida et al., 1989; Punshon

Jorge 4/1/15 10:58 AM

Deleted: reaction with OH radicals

Jorge 4/1/15 10:57 AM

Deleted: that

Jorge 4/1/15 2:43 PM

Deleted: 1995

92 and Moore, 2004; De Wilde and De Bic, 2000).

93 N<sub>2</sub>O is formed in the ocean interior through two major pathways and consumed only in  
94 oxygen minimum zones through denitrification (Zamora et al., 2012). The first  
95 production pathway is associated with nitrification (conversion of ammonia, NH<sub>4</sub><sup>+</sup>, into  
96 nitrate, NO<sub>3</sub><sup>-</sup>), and occurs when dissolved O<sub>2</sub> concentrations are above 20 μmol L<sup>-1</sup>. We  
97 subsequently refer to this pathway as the high-O<sub>2</sub> pathway. The second production  
98 pathway is associated with a series of processes when O<sub>2</sub> concentrations fall below ~5  
99 μmol L<sup>-1</sup> and involve a combination of nitrification and denitrification (hereinafter  
100 referred to as low-O<sub>2</sub> pathway) (Cohen and Gordon, 1978; Goreau et al., 1980; Elkins et  
101 al., 1978). As nitrification is one of the processes involved in the aerobic remineralization  
102 of organic matter, it occurs nearly everywhere in the global ocean with a global rate at  
103 least one order of magnitude larger than the global rate of water column denitrification  
104 (Gruber, 2008). A main reason is that denitrification in the water column is limited to  
105 the OMZs, which occupy only a few percent of the total ocean volume (Bianchi et al.,  
106 2012). This is also the only place in the water column where N<sub>2</sub>O is being consumed.

107 The two production pathways have very different N<sub>2</sub>O yields, i.e., fractions of nitrogen-  
108 bearing products that are transformed to N<sub>2</sub>O. For the high-O<sub>2</sub> pathway, the yield is  
109 typically rather low, i.e., only about 1 in several hundred molecules of ammonium  
110 escapes as N<sub>2</sub>O (Cohen and Gordon, 1979). In contrast, in the low-O<sub>2</sub> pathway, and  
111 particularly during denitrification, this fraction may go up to as high as 1:1, i.e., that all  
112 nitrate is turned into N<sub>2</sub>O (Tiedje, 1988). The relative contribution of the two pathways  
113 to global N<sub>2</sub>O production is not well established. Sarmiento and Gruber (2006)  
114 suggested that the two may be of equal importance, but more recent estimates suggest  
115 that the high-O<sub>2</sub> production pathway dominates global oceanic N<sub>2</sub>O production (Freing  
116 et al., 2012).

117 Two strategies have been pursued in the development of parameterizations for N<sub>2</sub>O  
118 production in global biogeochemical models. The first approach builds on the  
119 importance of the nitrification pathway and its close association with the aerobic  
120 remineralization of organic matter. As a result the production of N<sub>2</sub>O and the  
121 consumption of O<sub>2</sub> are closely tied to each other, leading to a strong correlation between  
122 the concentration of N<sub>2</sub>O and the apparent oxygen utilization (AOU). This has led to the  
123 development of two sets of parameterizations, one based on concentrations, i.e., directly

124 as a function of AOU (Butler et al., 1989) and the other based on the rate of oxygen  
125 utilization, i.e. OUR (Freing et al., 2009). Additional variables have been introduced to  
126 allow for differences in the yield, i.e., the ratio of N<sub>2</sub>O produced over oxygen consumed,  
127 such as temperature (Butler et al., 1989) or depth (Freing et al., 2009). In the second  
128 approach, the formation of N<sub>2</sub>O is modeled more mechanistically, and tied to both  
129 nitrification and denitrification by an O<sub>2</sub> dependent yield (Suntharalingam and  
130 Sarmiento, 2000; Nevison et al., 2003; Jin and Gruber, 2003). Since most models do not  
131 include nitrification explicitly, the formation rate is actually coupled directly to the  
132 remineralization of organic matter. Regardless of the employed strategy, all  
133 parameterizations depend to first order on the amount of organic matter that is being  
134 remineralized in the ocean interior, which is governed by the export of organic carbon to  
135 depth. The dependence of N<sub>2</sub>O production on oxygen levels and on other parameters  
136 such as temperature only acts at second order. This has important implications not only  
137 for the modeling of the present-day distribution of N<sub>2</sub>O in the ocean, but also for the  
138 sensitivity of marine N<sub>2</sub>O to future climate change.

139 Over this century, climate change will perturb marine N<sub>2</sub>O formation in multiple ways.  
140 Changes in productivity will drive changes in the export of organic matter to the ocean  
141 interior (Steinacher et al., 2010; Bopp et al., 2013) and hence affect the level of marine  
142 nitrification. Ocean warming might [change](#) the rate of N<sub>2</sub>O production during  
143 nitrification (Freing et al., 2012). Changes in carbonate chemistry (Bindoff et al., 2007)  
144 might cause changes in the C:N ratio of the exported organic matter (Riebesell et al.,  
145 2007), altering not only the rates of nitrification, but also the ocean interior oxygen levels  
146 (Gehlen et al., 2011). Finally, the expected general loss of oxygen (Keeling et al., 2010;  
147 Cocco et al., 2012; Bopp et al., 2013) could substantially affect N<sub>2</sub>O production [via both](#)  
148 [nitrifier denitrification and classic denitrification](#).

149 [Ocean biogeochemical models](#) used for IPCC's 4<sup>th</sup> assessment report estimated a decrease  
150 between 2% and 13% in primary production (PP) under the business-as-usual high CO<sub>2</sub>  
151 concentration scenario A2 (Steinacher et al., 2010). A more recent multi-model analysis  
152 based on the models used in IPCC's 5<sup>th</sup> assessment report also suggest a large reduction of  
153 PP down to 18% by 2100 for the RCP8.5 scenario (Bopp et al., 2013). In these  
154 simulations, the export of organic matter is projected to decrease between 6% and 18%  
155 in 2100 (Bopp et al., 2013), with a spatially distinct pattern: in general, productivity and

Jorge 4/1/15 10:54 AM

Deleted: increase

Jorge 4/1/15 10:53 AM

Deleted: denitrification and the

Jorge 4/1/15 10:52 AM

Deleted: M

159 export are projected to decrease at mid- to low-latitudes in all basins, while productivity  
160 and export are projected to increase in the high-latitudes and in the South Pacific  
161 subtropical gyre (Bopp et al., 2013). A wider spectrum of responses was reported  
162 regarding changes in the ocean oxygen content. While all models simulate decreased  
163 oxygen concentrations in response to anthropogenic climate change (by about 2 to 4% in  
164 2100), and particularly in the mid-latitude thermocline regions, no agreement exists with  
165 regard to the hypoxic regions, i.e., those having oxygen levels below  $60 \mu\text{mol L}^{-1}$  (Cocco  
166 et al., 2012; Bopp et al., 2013). Some models project these regions to expand, while  
167 others project a contraction. Even more divergence in the results exists for the suboxic  
168 regions, i.e., those having  $\text{O}_2$  concentrations below  $5 \mu\text{mol L}^{-1}$  (Keeling et al., 2010;  
169 Deutsch et al., 2011; Cocco et al., 2012; Bopp et al., 2013), although the trend for most  
170 models is pointing towards an expansion. At the same time, practically none of the  
171 models is able to correctly simulate the current distribution of oxygen in the OMZ (Bopp  
172 et al., 2013). In summary, while it is clear that major changes in ocean biogeochemistry  
173 are looming ahead (Gruber, 2011), with substantial impacts on the production and  
174 emission of  $\text{N}_2\text{O}$ , our ability to project these changes with confidence is limited.

175 In this study, we explore the implications of these future changes in ocean physics and  
176 biogeochemistry on the marine  $\text{N}_2\text{O}$  cycle, and make projections of the oceanic  $\text{N}_2\text{O}$   
177 emissions from year 2005 to 2100 under the high  $\text{CO}_2$  concentration scenario RCP8.5.  
178 We analyze how changes in biogeochemical and physical processes such as net primary  
179 production (NPP), export production and vertical stratification in this century translate  
180 into changes in oceanic  $\text{N}_2\text{O}$  emissions to the atmosphere. To this end, we use the  
181 NEMO-PISCES ocean biogeochemical model, which we have augmented with two  
182 different  $\text{N}_2\text{O}$  parameterizations, permitting us to evaluate changes in the marine  $\text{N}_2\text{O}$   
183 cycle at the process level, especially with regard to production pathways in high and low  
184 oxygen regimes. We demonstrate that while future changes in the marine  $\text{N}_2\text{O}$  cycle will  
185 be substantial, the net emissions of  $\text{N}_2\text{O}$  appear to change relatively little, i.e., they are  
186 projected to decrease by about 10% in 2100.

187

## 188 2. Methodology

189

### 190 2.1 NEMO-PISCES Model

191

192 Future projections of the changes in the oceanic N<sub>2</sub>O cycle were performed using the  
193 PISCES ocean biogeochemical model (Aumont and Bopp, 2006) in offline mode with  
194 physical forcings derived from the IPSL-CM5A-LR coupled model (Dufresne et al.,  
195 2013). The horizontal resolution of NEMO ocean general circulation model is 2° x 2° cos  
196 Ø (Ø being the latitude) with enhanced latitudinal resolution at the equator of 0.5°.  
197 PISCES is a biogeochemical model with five nutrients (NO<sub>3</sub>, NH<sub>4</sub>, PO<sub>4</sub>, Si and Fe), two  
198 phytoplankton groups (diatoms and nanophytoplankton), two zooplankton groups  
199 (micro and mesozooplankton), and two non-living compartments (particulate and  
200 dissolved organic matter). Phytoplankton growth is limited by nutrient availability and  
201 light. Constant Redfield C:N:P ratios of 122:16:1 are assumed (Takahashi et al., 1985),  
202 while all other ratios, i.e., those associated with chlorophyll, iron, and silicon (Chl:C,  
203 Fe:C and Si:C) vary dynamically.

204

205 2.2 N<sub>2</sub>O parameterizations in PISCES

206

207 We implemented two different parameterizations of N<sub>2</sub>O production in NEMO-PISCES.  
208 The first one, adapted from Butler et al. (1989) follows the oxygen consumption  
209 approach, with a temperature dependent modification of the N<sub>2</sub>O yield (P.TEMP). The  
210 second one is based on Jin and Gruber (2003) (P.OMZ), following the more mechanistic  
211 approach, i.e., it considers the different processes occurring at differing oxygen  
212 concentrations in a more explicit manner.

213 The P.TEMP parameterization assumes that the N<sub>2</sub>O production is tied to nitrification  
214 only with a yield that is at first order constant. This is implemented in the model by  
215 tying the N<sub>2</sub>O formation in a linear manner to O<sub>2</sub> consumption. A small temperature  
216 dependence is added to the yield to reflect the potential impact of temperature on  
217 metabolic rates. The production term of N<sub>2</sub>O, i.e.,  $J^{P.TEMP}(N_2O)$ , is then mathematically  
218 formulated as:

$$219 \quad J^{P.TEMP}(N_2O) = (\gamma + \theta T) J(O_2)_{consumption} \quad (1)$$

220 where  $\gamma$  is a background yield ( $0.53 \times 10^{-4}$  mol N<sub>2</sub>O/mol O<sub>2</sub> consumed),  $\theta$  is the  
221 temperature dependency of  $\gamma$  ( $4.6 \times 10^{-6}$  mol N<sub>2</sub>O (mol O<sub>2</sub>)<sup>-1</sup> K<sup>-1</sup>),  $T$  is temperature (K),

222 and  $J(O_2)_{consumption}$  is the sum of all biological  $O_2$  consumption terms within the model.  
223 The same ratio between constants  $\gamma$  and  $\theta$  is used in the model as in the original  
224 formulation from Butler et al. (1989). Although this parameterization is very simple, a  
225 recent analysis of  $N_2O$  observations supports such an essentially constant yield, even in  
226 the OMZ of the Eastern Tropical Pacific (Zamora et al., 2012).

227 The P.OMZ parameterization, formulated after Jin and Gruber (2003), assumes that the  
228 overall yield consists of a constant background yield and an oxygen dependent yield. The  
229 former is presumed to represent the  $N_2O$  production by nitrification, while the latter is  
230 presumed to reflect the enhanced production of  $N_2O$  at low oxygen concentrations, in  
231 part driven by denitrification, but possibly including nitrification as well. This  
232 parameterization includes the consumption of  $N_2O$  in suboxic conditions. This gives:

$$233 \quad J^{P.OMZ}(N_2O) = (\alpha + \beta f(O_2))J(O_2)_{consumption} - k N_2O \quad (2)$$

234 where  $\alpha$  is, as in Eq.(1), a background yield ( $0.9 \cdot 10^{-4}$  mol  $N_2O$ /mol  $O_2$  consumed),  $\beta$  is  
235 a yield parameter that scales the oxygen dependent function ( $6.2 \cdot 10^{-4}$ ),  $f(O_2)$  is a unitless  
236 oxygen-dependent step-like modulating function, as suggested by laboratory experiments  
237 (Goreau et al., 1980) (Fig. S1, Supplementary Material), and  $k$  is the 1<sup>st</sup> order rate  
238 constant of  $N_2O$  consumption close to anoxia (zero otherwise). For  $k$ , we have adopted a  
239 value of  $0.138 \text{ yr}^{-1}$  following Bianchi et al. (2012) while we set the consumption regime

240 for  $O_2$  concentrations below  $5 \mu\text{mol L}^{-1}$ . The constant  $\alpha$  is in the same order of  
241 magnitude as the one proposed by Jin and Gruber (2003), while  $\beta$  is two orders of  
242 magnitude smaller. The use of the original value would result in a significant increase of  
243  $N_2O$  production associated with OMZs and, hence, in a departure from the assumption  
244 of dominant nitrification.

245 The P.OMZ parameterization permits us the independent quantification of the  $N_2O$   
246 formation pathways associated with nitrification and those associated with low-oxygen  
247 concentrations (nitrification/denitrification) and their evolution in time over the next  
248 century. Specifically, we consider the source term  $\alpha J(O_2)_{consumption}$  as that associated with  
249 the nitrification pathway, while we associated the source term  $\beta f(O_2) J(O_2)_{consumption}$  with  
250 the low-oxygen processes (Fig. S2, Supplementary Material).

251  $N_2O$  production is inhibited by light in the model, and therefore  $N_2O$  production in  
252 P.TEMP and P.OMZ parameterizations only occurs below a fixed depth of 100m.

Jorge 4/1/15 12:54 PM

Deleted: to separately identify



254 We employ a standard bulk approach for simulating the loss of N<sub>2</sub>O to the atmosphere  
255 via gas exchange. We use the formulation of Wanninkhof et al. (1992) for estimating the  
256 gas transfer velocity, adjusting the Schmidt number for N<sub>2</sub>O and using the solubility  
257 constants of N<sub>2</sub>O given by Weiss and Price (1980). We assume a constant atmospheric  
258 N<sub>2</sub>O concentration of 284 ppb in all simulations to explore future changes inherent to  
259 ocean processes without feedbacks due to changes in the atmosphere.

260

### 261 2.3 Experimental design

262

263 NEMO-PISCES was first spun up during 3000 years using constant pre-industrial  
264 dynamical forcings fields from IPSL-CM5A-LR (Dufresne et al., 2013) without  
265 activating the N<sub>2</sub>O parameterizations. This spin-up phase was followed by a 150-yr long  
266 simulation, forced by the same dynamical fields now with N<sub>2</sub>O production and N<sub>2</sub>O sea-  
267 to-air flux embedded. The N<sub>2</sub>O concentration at all grid points was prescribed initially to  
268 20 nmol L<sup>-1</sup>, which is consistent with the MEMENTO database average value of 18  
269 nmol L<sup>-1</sup> below 1500m (Bange et al., 2009). During the 150-yr spin-up, we diagnosed  
270 the total N<sub>2</sub>O production and N<sub>2</sub>O sea-to-air flux and adjusted the  $\alpha$ ,  $\beta$ ,  $\gamma$  and  $\theta$   
271 parameters in order to achieve a total N<sub>2</sub>O sea-to-air flux in the two parameterizations at  
272 equilibrium close to 3.85 TgN yr<sup>-1</sup> (Ciais et al., 2013). In addition, the relative  
273 contribution of the high-O<sub>2</sub> pathway in the P.OMZ parameterization was set to 75% of  
274 the total N<sub>2</sub>O production based on Suntharalingam et al. (2000), where a sensitivity  
275 model analysis on the relative contribution of high- and low-O<sub>2</sub> production pathways  
276 showed that a higher contribution of nitrification (75%) than denitrification (25%)  
277 achieved the best model performance compared to the data product from Nevison et al.  
278 (1995). P.TEMP can be considered as 100% nitrification, testing in this way the  
279 hypothesis of nitrification as the dominant pathway of N<sub>2</sub>O production on a global scale.  
280 Nitrification could contribute with up to 93% of the total production based on  
281 estimations considering N<sub>2</sub>O production along with water mass transport (Freing et al.,  
282 2012).

283 Projections in NEMO-PISCES of historical (from 1851 to 2005) and future (from 2005  
284 to 2100) simulated periods were done using dynamical forcing fields from IPSL-CM5A-  
285 LR. These dynamical forcings were applied in an offline mode, i.e. monthly means of

Jorge 4/1/15 12:53 PM

Deleted: This

Jorge 4/1/15 12:53 PM

Deleted: assumption is based on growing evidence

Jorge 4/3/15 2:28 PM

Deleted: that

Jorge 4/3/15 2:28 PM

Deleted: is

Jorge 4/3/15 2:27 PM

Deleted: ,

292 temperature, velocity, wind speed or radiative flux were used to force NEMO-PISCES.  
293 Future simulations used the business-as-usual high CO<sub>2</sub> concentration scenario (RCP8.5)  
294 until year 2100. Century scale model drifts for all the biogeochemical variables presented,  
295 including N<sub>2</sub>O sea-to-air flux, production and inventory, were removed using an  
296 additional control simulation with IPSL-CM5A-LR pre-industrial dynamical forcing  
297 fields from year 1851 to 2100. Despite the fact that primary production and the export  
298 of organic matter to depth were stable in the control simulation, the air-sea N<sub>2</sub>O  
299 emissions drifted (an increase of 5 to 12% in 200 yr depending on the parameterization)  
300 due to the short spin-up phase (150 yrs) and to the choice of the initial conditions for  
301 N<sub>2</sub>O concentrations.

302

### 303 3. Present-day oceanic N<sub>2</sub>O

304

#### 305 3.1 Contemporary N<sub>2</sub>O fluxes

306

307 The model simulated air-sea N<sub>2</sub>O emissions show large spatial contrasts, with flux  
308 densities varying by one order of magnitude, but with relatively small differences between  
309 the two parameterizations (Fig. 1a and 1b). This is largely caused by our assumption that  
310 the dominant contribution (75%) to the total N<sub>2</sub>O production in the P.OMZ  
311 parameterization is the nitrification pathway, which is then not so different from the  
312 P.TEMP parameterization, where it is 100%. As a result, the major part of N<sub>2</sub>O is  
313 produced [in](#) the subsurface via nitrification, contributing directly to imprint changes into  
314 the sea-to-air N<sub>2</sub>O flux without a significant meridional transport (Suntharalingam and  
315 Sarmiento, 2000).

316 Elevated N<sub>2</sub>O emission regions (> 50 mgN m<sup>-2</sup> yr<sup>-1</sup>) are found in the [Equatorial and](#)  
317 [Eastern Tropical Pacific](#), in the northern Indian ocean, in the northwestern Pacific, in the  
318 North Atlantic and in the Agulhas Current. In contrast, low fluxes (< 10 mgN m<sup>-2</sup> yr<sup>-1</sup>)  
319 are simulated in the [Southern Ocean](#), Atlantic and Pacific subtropical gyres and southern  
320 Indian Ocean. [The large scale distribution of N<sub>2</sub>O fluxes is coherent with Nevison et al.](#)  
321 [\(2004\) \(Fig. 1c\)](#). This comes as a natural consequence of the relatively high contribution  
322 of nitrification and hence hotspots of N<sub>2</sub>O emissions are associated with regions where  
323 higher export of organic matter occurs in the model.

Jorge 3/31/15 3:08 PM

Deleted: close to

325 There are however several discrepancies between the model and the data product. At high  
326 latitudes, the high N<sub>2</sub>O emissions observed in the North Pacific are not well represented  
327 in our model, with a significant shift towards the western part of the Pacific basin, similar  
328 to other modeling studies (e.g., Goldstein et al., 2003; Jin and Gruber, 2003). The OMZ  
329 in the North Pacific, located at approximately 600m deep, is underestimated in the  
330 model due to the deficient representation of the Meridional Overturning Circulation  
331 (MOC) in the North Pacific in global ocean biogeochemical models, which in turn  
332 might suppress low oxygenated areas and therefore one potential N<sub>2</sub>O source.  
333 Discrepancies between model and observations also occur in the Southern Ocean, a  
334 region whose role in global N<sub>2</sub>O fluxes remains debated due to the lack of observations  
335 and the occurrence of potential artifacts due to interpolation techniques reflected in data  
336 products such as that from Nevison et al., 2004. (e.g., Suntharalingam and Sarmiento,  
337 2000, and Nevison et al, 2003). The model also overestimates N<sub>2</sub>O emissions in the  
338 North Atlantic. The emphasis put on the nitrification pathway suggests that hotspots of  
339 carbon export are at the origin of elevated concentrations of N<sub>2</sub>O in the subsurface. N<sub>2</sub>O  
340 is quickly outgassed to the atmosphere, leading to such areas of high N<sub>2</sub>O emissions in  
341 the model.

342 Model-data discrepancies can be seen as a function of latitude in Figure 1d. The modeled  
343 N<sub>2</sub>O flux maxima peak at around 40°S, i.e., around 10° north to that estimated by  
344 Nevison et al. (2004), although Southern Ocean data must be interpreted with caution.  
345 In the northern hemisphere the stripe in the North Pacific is not captured by the model,  
346 splitting the flux from the 45°N band into two peaks at 38°N and 55°N.

### 347 3.2 Contemporary N<sub>2</sub>O concentrations and the relationship to O<sub>2</sub>

348  
349  
350 The model results at present day were evaluated against the MEMENTO database  
351 (Bange et al., 2009), which contains about 25,000 measurements of co-located N<sub>2</sub>O and  
352 dissolved O<sub>2</sub> concentrations. Table 1 summarizes the standard deviation and correlation  
353 coefficients for P.TEMP and P.OMZ compared to MEMENTO. The standard deviation  
354 of the model output is very similar to MEMENTO, i.e., around 16 nmol L<sup>-1</sup> of N<sub>2</sub>O.  
355 However, the correlation coefficients between the sampled data points from  
356 MEMENTO and P.TEMP / P.OMZ are 0.49 and 0.42 respectively. Largest

Jorge 4/1/15 11:13 AM

**Deleted:** The regions of high N<sub>2</sub>O emissions are in both parameterizations generally consistent with the data product of Nevison et al. (1995) (Fig. 1c), especially in the equatorial latitudes. The largest discrepancies occur in the North Pacific and Southern Ocean.

Jorge 4/1/15 11:08 AM

**Deleted:** The high

Jorge 4/1/15 11:09 AM

**Deleted:** by

Jorge 4/1/15 11:09 AM

**Deleted:** in the North Pacific

Jorge 4/1/15 11:10 AM

**Deleted:** might be

Jorge 4/1/15 11:10 AM

**Deleted:** our

Jorge 4/1/15 11:11 AM

**Deleted:** Minor d

Jorge 4/1/15 11:18 AM

**Deleted:** In particular, t

Jorge 4/1/15 11:18 AM

**Deleted:** 1995

Jorge 4/1/15 11:18 AM

**Deleted:** (Fig. 1d

Jorge 4/1/15 11:18 AM

**Deleted:** ).

373 discrepancies are found mostly in the deep ocean and in the OMZs.  
374 Figure 2 compares the global average vertical profile of the observed N<sub>2</sub>O against the  
375 results from the two parameterisations. The in-situ observations show three characteristic  
376 layers: the upper 100m layer with low (~10 nmol L<sup>-1</sup>) N<sub>2</sub>O concentration due to gas  
377 exchange keeping N<sub>2</sub>O close to its saturation concentration, the mesopelagic layer,  
378 between 100 and 1500m, where N<sub>2</sub>O is enriched via nitrification and denitrification in  
379 the OMZs, and the deep ocean beyond 1500m, with a relatively constant concentration  
380 of 18 nmol L<sup>-1</sup> on average. Both parameterizations underestimate the N<sub>2</sub>O concentration  
381 in the upper 100 meters, where most of the N<sub>2</sub>O is potentially outgassed to the  
382 atmosphere. In the second layer, P.OMZ shows a fairly good agreement with the  
383 observations in the 500 to 900m band, whereas P.TEMP is too low by ~10 nmol L<sup>-1</sup>.  
384 Below 1500m, both parameterizations simulate too high N<sub>2</sub>O compared to the  
385 observations. This may be caused by the lack or underestimation of a sink process in the  
386 deep ocean, or by the too high concentrations used to initialize the model, which persist  
387 due to the rather short spin-up time of only 150 yrs.  
388 The analysis of the model simulated N<sub>2</sub>O concentrations as a function of model  
389 simulated O<sub>2</sub> shows the differences between the two parameterizations more clearly (Fig.  
390 3a and 3b). Such a plot allows us to assess the model performance with regard to N<sub>2</sub>O  
391 (Jin and Gruber, 2003), without being subject to the strong potential biases introduced  
392 by the model's deficiencies in simulating the distribution of O<sub>2</sub>. This is particularly  
393 critical in the OMZs, where all models exhibit strong biases (Cocco et al., 2012; Bopp et  
394 al., 2013) (see also Fig. 3c). P.TEMP (Fig. 3a) slightly overestimates N<sub>2</sub>O for dissolved  
395 O<sub>2</sub> concentrations above 100 μmol L<sup>-1</sup>, and does not fully reproduce either the high N<sub>2</sub>O  
396 values in the OMZs or the N<sub>2</sub>O depletion when O<sub>2</sub> is almost completely consumed.  
397 P.OMZ (Figure 3b) overestimates the N<sub>2</sub>O concentration over the whole range of O<sub>2</sub>,  
398 with particularly high values of N<sub>2</sub>O above 100 nmol L<sup>-1</sup> due to the exponential function  
399 used in the OMZs. There, the observations suggest concentrations below 80 nmol L<sup>-1</sup> for  
400 the same low O<sub>2</sub> values, consistent with the linear trend observed for higher O<sub>2</sub>, which  
401 seems to govern over most of the O<sub>2</sub> spectrum, as suggested by Zamora et al. (2012). The  
402 discrepancy at low O<sub>2</sub> concentration may also stem from our choice of a too low N<sub>2</sub>O  
403 consumption rate under essentially anoxic conditions. Finally, it should be considered  
404 that most of the MEMENTO data points are from OMZs and therefore N<sub>2</sub>O

Jorge 4/1/15 10:59 AM

Deleted: good correlation

Jorge 3/31/15 3:09 PM

Deleted: n

Jorge 3/31/15 3:09 PM

Deleted: n

Jorge 4/3/15 2:11 PM

**Moved down [1]:** The O<sub>2</sub> distribution in the model (Fig. 3c) shows a deficient representation of the OMZs, with higher concentrations than those from observations in the oxygen-corrected World Ocean Atlas (Bianchi et al., 2012). The rest of the O<sub>2</sub> spectrum is well represented in our model.

415 measurements could be biased towards higher values than the actual open ocean average,  
416 where our model performs better.

417

#### 418 4. Future oceanic N<sub>2</sub>O

419

##### 420 4.1 N<sub>2</sub>O sea-to-air flux

421

422 The global oceanic N<sub>2</sub>O emissions decrease relatively little over the next century (Fig. 4a)  
423 between 4% and 12%. Namely, in P.TEMP, the emissions decrease by 0.15 TgN yr<sup>-1</sup>  
424 from 3.71 TgN yr<sup>-1</sup> in 1985-2005 to 3.56 TgN yr<sup>-1</sup> in 2080-2100 and in P.OMZ, the  
425 decrease is slightly larger at 12%, i.e., amounting to 0.49 Tg N yr<sup>-1</sup> from 4.03 to 3.54  
426 TgN yr<sup>-1</sup>. Notable is also the presence of a negative trend in N<sub>2</sub>O emissions over the 20<sup>th</sup>  
427 century, most pronounced in the P.OMZ parameterization. Considering the change over  
428 the 20<sup>th</sup> and 21<sup>st</sup> centuries together, the decreases increase to 7 and 15%.

429 These relatively small global decreases mask more substantial changes at the regional scale,  
430 with a mosaic of regions experiencing a substantial increase and regions experiencing a  
431 substantial decrease (Fig. 4b and 4c). In both parameterizations, the oceanic N<sub>2</sub>O  
432 emissions decrease in the northern and south western oceanic basins (e.g., the North  
433 Atlantic and Arabian Sea), by up to 25 mgN m<sup>-2</sup>yr<sup>-1</sup>. In contrast, the fluxes are simulated  
434 to increase in the Eastern Tropical Pacific and in the Bay of Bengal. For the Benguela  
435 Upwelling System (BUS) and the North Atlantic a bi-modal pattern emerges in 2100. As  
436 was the case for the present-day distribution of the N<sub>2</sub>O fluxes, the overall similarity  
437 between the two parameterizations is a consequence of the dominance of the nitrification  
438 (high-O<sub>2</sub>) pathway in both parameterizations.

439 Nevertheless there are two regions where more substantial differences between the two  
440 parameterizations emerge: the region overlying the oceanic OMZ at the BUS and the  
441 Southern Ocean. In particular, the P.TEMP parameterization projects a larger  
442 enhancement of the flux than P.OMZ at the BUS, whereas the emissions in the Southern  
443 Ocean are enhanced in the P.OMZ parameterization.

444

##### 445 4.2 Drivers of changes in N<sub>2</sub>O emissions

446

447 The changes in N<sub>2</sub>O emissions may stem from a change in net N<sub>2</sub>O production, a change  
448 in the transport of N<sub>2</sub>O from its location of production to the surface, or any  
449 combination of the two, which includes also changes in N<sub>2</sub>O storage. Next we determine  
450 the contribution of these mechanisms to the overall decrease in N<sub>2</sub>O emissions that our  
451 model simulated for the 21<sup>st</sup> century.

452

#### 453 4.2.1 Changes in N<sub>2</sub>O production

454

455 In both parameterizations, global N<sub>2</sub>O production is simulated to decrease over the 21<sup>st</sup>  
456 century. The total N<sub>2</sub>O production in P.OMZ decreases by 0.41 TgN yr<sup>-1</sup> in 2080-2100  
457 compared to the mean value over 1985-2005 (Fig. 5a). The parameterization P.OMZ  
458 allows to isolate the contributions of high- and low-O<sub>2</sub> and will be analysed in greater  
459 detail in the following sections. N<sub>2</sub>O production via the high-O<sub>2</sub> pathway in P.OMZ  
460 decreases in the same order than total production, by 0.35 TgN yr<sup>-1</sup> in 2080-2100  
461 compared to present. The N<sub>2</sub>O production in the low-O<sub>2</sub> regions remains almost  
462 constant across the experiment. In P.TEMP parameterization, the reduction in N<sub>2</sub>O  
463 production is much weaker than in P.OMZ due to the effect of the increasing  
464 temperature. N<sub>2</sub>O production decreases by 0.07 TgN yr<sup>-1</sup> in 2080-2100 compared to  
465 present (Fig. 5b).

466 The vast majority of the changes in the N<sub>2</sub>O production in the P.OMZ parameterization  
467 is caused by the high-O<sub>2</sub> pathway with virtually no contribution from the low-O<sub>2</sub>  
468 pathway (Fig. 5a). As the N<sub>2</sub>O production in [P.OMZ parameterization](#) is solely driven  
469 by changes in the O<sub>2</sub> consumption (Eq. (2)), which in our model is directly linked to  
470 export production, the dominance of this pathway implies that primary driver for the  
471 future changes in N<sub>2</sub>O production in our model is the decrease in export of organic  
472 matter (CEX). It was simulated to decrease by 0.97 PgC yr<sup>-1</sup> in 2100, and the high degree  
473 of correspondence in the temporal evolution of export and N<sub>2</sub>O production in Fig. 5a  
474 confirms this conclusion.

475 The close connection between N<sub>2</sub>O production associated with the high-O<sub>2</sub> pathway and  
476 changes in export production is also seen spatially (Fig. 5c), where the spatial pattern of  
477 changes in export and changes in N<sub>2</sub>O production are extremely highly correlated (shown  
478 by stippling). Most of the small deviations are caused by lateral advection of organic

Jorge 4/1/15 10:45 AM

Deleted: this pathway

Jorge 3/31/15 2:43 PM

Deleted: see

481 carbon, causing a spatial separation between changes in O<sub>2</sub> consumption and changes in  
482 organic matter export.

483 As there is an almost ubiquitous decrease of export in all of the major oceanic basins  
484 except at high latitudes, N<sub>2</sub>O production decreases overall as well. Hotspots of reductions  
485 exceeding -10 mgN m<sup>-2</sup>yr<sup>-1</sup> are found in the North Atlantic, the western Pacific and  
486 Indian basins (Fig. 5c). The fewer places where export increases, are also the locations of  
487 enhanced N<sub>2</sub>O production. For example, a moderate increase of 3 mgN m<sup>-2</sup> yr<sup>-1</sup> is  
488 projected in the Southern Ocean, South Atlantic and Eastern Tropical Pacific. The  
489 general pattern of export changes, i.e., decreases in lower latitudes, increase in higher  
490 latitudes, is consistent generally with other model projection patterns (Bopp et al., 2013),  
491 although there exist very strong model-to-model differences at the more regional scale.

492 Although the global contribution of the changes in the low-O<sub>2</sub> N<sub>2</sub>O production is small,  
493 this is the result of regionally compensating trends. In the model's OMZs, i.e., in the  
494 Eastern Tropical Pacific and in the Bay of Bengal, a significant increase in N<sub>2</sub>O  
495 production is simulated in these locations (Fig. 5d), with an increase of more than 15  
496 mgN m<sup>-2</sup> yr<sup>-1</sup>. This increase is primarily driven by the expansion of the OMZs in our  
497 model (shown by stippling), while changes in export contribute less. In effect, NEMO-  
498 PISCES projects a 20% increase in the hypoxic volume globally, from 10.2 to 12.3 x 10<sup>6</sup>  
499 km<sup>3</sup>, and an increase in the suboxic volume from 1.1 to 1.6 x 10<sup>6</sup> km<sup>3</sup> in 2100 (Fig. 5e).  
500 Elsewhere, the changes in the N<sub>2</sub>O production through the low-O<sub>2</sub> pathway are  
501 dominated by the changes in export, thus following the pattern of the changes seen in the  
502 high-O<sub>2</sub> pathway. Overall these changes are negative, and happen to nearly completely  
503 compensate the increase in production in the OMZs, resulting in the near constant  
504 global N<sub>2</sub>O production by the low-O<sub>2</sub> production pathway up to year 2100.

505

#### 506 4.2.2 Changes in storage of N<sub>2</sub>O

507

508 A steady increase in the N<sub>2</sub>O inventory is observed from present to 2100. The pool of  
509 oceanic N<sub>2</sub>O down to 1500m, i.e., potentially outgassed to the atmosphere, increases by  
510 8.9 TgN from 1985-2005 to year 2100 in P.OMZ, whereas P.TEMP is less sensitive to  
511 changes with an increase of 4.0 TgN on the time period considered (Fig. 6a). [The](#)  
512 [inventory in the upper 1500m in P.OMZ is 237.0 TgN at present, while in P.TEMP in](#)

513 | the same depth band is 179.8 TgN. This means that the projected changes in the  
514 | inventory represent an increase of about 4% and 2% in P.OMZ and P.TEMP  
515 | respectively.

516 | This increase in storage of N<sub>2</sub>O in the ocean interior shows an homogeneous pattern for  
517 | P.TEMP, with particular hotspots in the North Pacific, North Atlantic and the eastern  
518 | boundary currents in the Pacific (Fig. 6b). The spatial variability is more pronounced in  
519 | P.OMZ (Fig. 6c), related in part to the enhanced production associated with OMZs.  
520 | Most of the projected changes in storage are associated with shoaling of the mixed layer  
521 | depth (shown by stippling), suggesting that increase in N<sub>2</sub>O inventories is caused by  
522 | increased ocean stratification. Enhanced ocean stratification, in turn, occurs in response  
523 | to increasing sea surface temperatures associated with global warming (Sarmiento et al.,  
524 | 2004).

525

#### 526 | 4.2.3 Effects of the combined mechanisms on N<sub>2</sub>O emissions

527

528 | The drivers of the future evolution of oceanic N<sub>2</sub>O emissions emerge from the preceding  
529 | analysis. Firstly, a decrease in the high-O<sub>2</sub> production pathway driven by a reduced  
530 | organic matter remineralization reduces N<sub>2</sub>O concentrations below the euphotic zone.  
531 | Secondly, the increased N<sub>2</sub>O inventory at depth is caused by increased stratification and  
532 | therefore to a less efficient transport to the sea-to-air interface, leading to a less N<sub>2</sub>O flux.

533 | The global changes in N<sub>2</sub>O flux, N<sub>2</sub>O production and N<sub>2</sub>O storage for P.OMZ are  
534 | presented in Fig. 7. Changes in N<sub>2</sub>O flux and N<sub>2</sub>O production are mostly of the same  
535 | sign in almost all of the oceanic regions in line with the assumption of nitrification being

536 | the dominant contribution to N<sub>2</sub>O production. Changes in N<sub>2</sub>O production in the  
537 | subsurface are translated into corresponding changes in N<sub>2</sub>O flux. There is only one  
538 | oceanic region (Sub-Polar Pacific) where this correlation does not occur. N<sub>2</sub>O inventory  
539 | increases in all of the oceanic regions. The increase in inventory is particularly  
540 | pronounced at low latitudes along the eastern boundary currents in the Equatorial and  
541 | Tropical Pacific, Indian Ocean and also in smaller quantities in the Atlantic Ocean.

542 | Figure 7 shows how the decrease in N<sub>2</sub>O production and increase in N<sub>2</sub>O storage occurs  
543 | in all oceanic basins.

544 | The synergy among the driving mechanisms can be explored with a box model pursuing

Jorge 3/31/15 3:08 PM

Deleted: close to

Jorge 3/31/15 3:05 PM

Deleted: almost all the relevant changes

Jorge 3/31/15 3:06 PM

Deleted: are related to low-latitude processes, with little or no contribution from changes in polar regions.



550 two objectives. First, to separate the effect of physical (i.e., increased stratification) and  
 551 the biogeochemical (i.e., reduction of N<sub>2</sub>O production in the high-O<sub>2</sub> regions)  
 552 mechanisms on N<sub>2</sub>O emissions. In this way we can reproduce future projections  
 553 assuming that the only mechanisms ruling the N<sub>2</sub>O dynamics in the future were those  
 554 that we have proposed in our hypothesis, i.e., increased stratification and reduction of  
 555 N<sub>2</sub>O production in high-O<sub>2</sub> regions. Secondly, to explore a wider range of values for both  
 556 mixing (i.e., degree of stratification) and efficiency of N<sub>2</sub>O production in high-O<sub>2</sub>  
 557 conditions. In the particular NEMO-PISCES model projection we have studied, changes  
 558 in mixing and export are unique and can not be explored individually.

559 To this end, a box model was designed to explore the response of oceanic N<sub>2</sub>O emissions  
 560 to changes in export of organic matter (hence N<sub>2</sub>O production only in high-O<sub>2</sub>  
 561 conditions) and changes in the mixing ratio between deep (> 100m) and surface (< 100m)  
 562 layers. We divided the water column into two compartments: a surface layer in the upper  
 563 100m where 80% of surface N<sub>2</sub>O concentration is outgassed to the atmosphere (Eq. (3)),  
 564 and a deeper layer beyond 100m, where N<sub>2</sub>O is produced from remineralization as a  
 565 fraction of the organic matter exported in the ocean interior (Eq. (4)). The N<sub>2</sub>O  
 566 reservoirs in the surface and in the deep layer are allowed to exchange. The exchange is  
 567 regulated by a mixing coefficient  $v$ :

$$\text{surface N}_2\text{O}; \quad \frac{dN_2O^s}{dt} = -v \cdot (N_2O^s - N_2O^d) - \kappa \cdot N_2O^s \quad (3)$$

$$\text{deep N}_2\text{O}; \quad \frac{dN_2O^d}{dt} = v \cdot (N_2O^s - N_2O^d) + \epsilon \cdot \Phi^{POC} \quad (4)$$

568 where  $N_2O^s$  is N<sub>2</sub>O in the surface,  $N_2O^d$  is N<sub>2</sub>O in the deep reservoir,  $\Phi^{POC}$  is the flux of  
 569 POC into the lower compartment,  $v$  is the mixing coefficient between both  
 570 compartments,  $\kappa$  is the fraction of N<sub>2</sub>O<sup>s</sup> outgassed to the atmosphere and  $\epsilon$  the fraction of  
 571 POC leading to N<sub>2</sub>O<sup>d</sup> formation (Fig. S3 and Table S1, Supplementary Material).  
 572 Equations (3) and (4) are solved for a combination of POC fluxes and mixing coefficients,  
 573 reflecting the increasing stratification and the decrease in export production projected by  
 574 year 2100 (Sarmiento et al., 2004; Bopp et al., 2013).

575 A decrease in the N<sub>2</sub>O flux is observed for a wide range of boundary conditions  
 576 simulating reduced mixing and export of POC (Fig. 8a). The most extreme scenario  
 577 explored with the box model suggests a -20% decrease in N<sub>2</sub>O flux, although these

Jorge 4/1/15 10:41 AM

Deleted: to

Jorge 4/1/15 10:39 AM

Deleted: 4

Jorge 3/31/15 2:44 PM

Deleted: s

Jorge 4/1/15 10:39 AM

Deleted: 5

Jorge 4/1/15 10:39 AM

Deleted:

Jorge 3/31/15 2:44 PM

Deleted: 4

Jorge 3/31/15 2:44 PM

Deleted: 5

Jorge 3/31/15 2:44 PM

Deleted: 4

Jorge 3/31/15 2:44 PM

Deleted: 5

Jorge 4/1/15 5:17 PM

Deleted: The equivalent of the transient NEMO-PISCES simulation, i.e., a -10% decrease in N<sub>2</sub>O flux, is achieved for a -8% decrease in export in the box model.

591 associated values of mixing and export are clearly unrealistic, from a nearly total  
592 stagnation of ocean circulation between the deep and surface layers to an attenuation of  
593 export of -20% in the global ocean.

594 The projected increase in N<sub>2</sub>O storage in the deep reservoir is reproduced by the box  
595 model (Fig. 8b) at a wide range of changes particularly in mixing. Changes in mixing  
596 dominate over changes in export as drivers of the increase in the N<sub>2</sub>O reservoir at depth.  
597 A 25% decrease in mixing leads to an increase in storage similar to the one projected with  
598 NEMO-PISCES (+10%), independently of changes in export of organic matter.

599 In general, the interplay between mixing and export of organic matter operates differently  
600 when N<sub>2</sub>O flux or N<sub>2</sub>O inventory are considered. The box model experiment suggests  
601 that the evolution of the N<sub>2</sub>O reservoir is driven almost entirely by changes in mixing,  
602 while changes of mixing and export of organic matter have similar relevance when  
603 modulating N<sub>2</sub>O emissions.

604

#### 605 5. Caveats in estimating N<sub>2</sub>O using ocean biogeochemical models

606

607 The state variables upon which representation of N<sub>2</sub>O in models rely, i.e., oxygen and  
608 export of carbon, are compared to the CMIP5 model ensemble to put our analysis in  
609 context of the current state-of-the-art model capabilities. We focus here our analysis on  
610 suboxic waters (O<sub>2</sub> < 5 μmol L<sup>-1</sup>) and on export production. Whereas CMIP5 models  
611 tend to have large volumes of O<sub>2</sub> concentrations in the suboxic regime, it is not the case  
612 for our NEMO-PISCES simulation, which clearly underestimates the volume of low-  
613 oxygen waters as compared to the oxygen corrected World Ocean Atlas 2005  
614 (WOA2005\*) (Bianchi et al., 2012). The fact that NEMO-PISCES forced by IPSL-  
615 CM5A-LR is highly oxygenated is confirmed by Figure 9, where the histogram of the full  
616 O<sub>2</sub> spectrum of WOA2005\* and NEMO-PISCES is shown. The O<sub>2</sub> distribution in the  
617 model shows a deficient representation of the OMZs, with higher concentrations than  
618 those from observations. The rest of the O<sub>2</sub> spectrum is well represented in our model.

619 The O<sub>2</sub> distribution in the model (Fig. 10) shows a deficient representation of the OMZs,  
620 with higher concentrations than those from observations in WOA2005\* and the other  
621 CMIP5 models. NEMO-PISCES is therefore biased towards the high O<sub>2</sub> production  
622 pathway of N<sub>2</sub>O due to the modeled O<sub>2</sub> fields.

Jorge 4/3/15 2:11 PM

Moved (insertion) [1]

Jorge 4/3/15 2:13 PM

Deleted: (Fig. 3c)

Jorge 4/3/15 2:15 PM

Deleted: in the oxygen-corrected World Ocean Atlas (Bianchi et al., 2012)

626 When turning to the export of organic matter, NEMO-PISCES is close to the CMIP5  
627 average value of 6.9 PgC yr<sup>-1</sup>. The overall distribution of export is also very similar to the  
628 CMIP5 model mean and both show smaller values than those from the data-based  
629 estimate of 9.84 PgC yr<sup>-1</sup> from Dunne et al., 2007 (Fig. 10).

630 The uncertainties derived from present and future model projections can be estimated  
631 using the spread in the CMIP5 model projection of export of organic matter and  
632 assuming a linear response between nitrification (or export) and N<sub>2</sub>O production in the  
633 subsurface, which is assumed to be quickly outgassed to the atmosphere. In NEMO-  
634 PISCES, a decrease in 13% in export leads to a maximum decrease in N<sub>2</sub>O emissions of  
635 12% in the P.OMZ scenario. Based on results by Bopp et al. (2013), changes in export of  
636 carbon span -7% to -18% in the CMIP5 model ensemble at the end of the 21st century  
637 and for RCP8.5. The spread would propagate to a similar range in projected N<sub>2</sub>O  
638 emissions across the CMIP5 model ensemble. Applying these values to present N<sub>2</sub>O  
639 emissions of 3.6 TgN yr<sup>-1</sup>, uncertainties are then bracketed between -0.25 and -0.65 TgN  
640 yr<sup>-1</sup>.

641 Regarding the low-O<sub>2</sub> pathway, a similar approach is not that straight forward. Zamora et  
642 al., (2012) found that a linear relationship between AOU and N<sub>2</sub>O production might  
643 occur even at the OMZ of the ETP. Zamora et al. (2012) acknowledged the fact that the  
644 MEMENTO database includes N<sub>2</sub>O advected from other regions and that mixing could  
645 play a relevant role, smoothing the fit between N<sub>2</sub>O and AOU from exponential to linear.  
646 However, Zamora et al. (2012) quoting Frame and Casciotti (2010), suggested that  
647 regions where an exponential relationship in N<sub>2</sub>O production is present might be rare, that  
648 other non-exponential N<sub>2</sub>O production processes might occur and therefore the plot they  
649 presented could describe the actual linear relationship between N<sub>2</sub>O production and  
650 oxygen consumption. Based on this hypothesis, we could refer again to the linear  
651 relationship suggested in the high-O<sub>2</sub> and export scenario. However, in this case the  
652 CMIP5 model projections of changes in the hypoxic and suboxic volumes differ  
653 substantially. Most models project an expansion of the OMZs in the +2% to +16% range  
654 in the suboxic volume (O<sub>2</sub> < 5 μmol L<sup>-1</sup>). There are, however, models that project a slight  
655 reduction of 2%. Spatial variability of projections add to the spread between CMIP5  
656 models. These discrepancies suggest that uncertainties from this spread must be  
657 interpreted with caution when estimating potential future N<sub>2</sub>O emissions.

658 The use of O<sub>2</sub> consumption as a proxy for the actual N<sub>2</sub>O production plays therefore a  
659 pivotal role in the uncertainties in N<sub>2</sub>O model estimations. Future model development  
660 should aim at the implementation of mechanistic parameterizations of N<sub>2</sub>O production  
661 based on nitrification and denitrification rates. Further, in order to determine accurate  
662 O<sub>2</sub> boundaries for both N<sub>2</sub>O production and N<sub>2</sub>O consumption at the core of OMZs  
663 additional measurements and microbial experiments are needed. The contribution of the  
664 high-O<sub>2</sub> pathway that was considered in this model analysis might be a conservative  
665 estimate. Freing et al. (2012) suggested that the high-O<sub>2</sub> pathway could be responsible of  
666 93% of the total N<sub>2</sub>O production. Assuming that changes in the N<sub>2</sub>O flux are mostly  
667 driven by N<sub>2</sub>O production via nitrification, that would suggest a larger reduction in the  
668 marine N<sub>2</sub>O emissions in the future. However, the mismatch between NEMO-PISCES  
669 and the Nevison et al. (2004) spatial distribution of N<sub>2</sub>O emissions in the western part of  
670 the basins suggests that changes in the future might not be as big as those projected in the  
671 model in such regions. Changes would be then distributed more homogeneously.

672 The model assumption neglecting N<sub>2</sub>O production in the upper 100m avoids one  
673 important source of uncertainty in estimating global oceanic N<sub>2</sub>O fluxes. In case  
674 nitrification occurs in the euphotic layer, our results would be facing a significant  
675 uncertainty of at least ±25% in N<sub>2</sub>O emissions according to Zamora and Oschlies (2014)  
676 analysis using the UVic Earth System Climate Model. Finally, Zamora et al. (2012)  
677 observed a higher than expected N<sub>2</sub>O consumption at the core of the OMZ in the  
678 Eastern Tropical Pacific, occurring at an upper threshold of 10 μmol L<sup>-1</sup>. The  
679 contribution of OMZs to total N<sub>2</sub>O production remains an open question. N<sub>2</sub>O  
680 formation associated with OMZs might be counterbalanced by its own local  
681 consumption, leading to the attenuation of the only increasing source of N<sub>2</sub>O  
682 attributable to the projected future expansion of OMZs (Steinacher et al., 2010; Bopp et  
683 al., 2013).

684 The combined effect of climate change and ocean acidification has not been analyzed in  
685 this study. N<sub>2</sub>O production processes might be altered by the response of nitrification to  
686 increasing levels of seawater pCO<sub>2</sub> (Huesemann et al., 2002; Beman et al. 2011). Beman  
687 et al. (2011) reported a reduction in nitrification in response to decreasing pH. This  
688 result suggests that N<sub>2</sub>O production might decrease beyond what we have estimated only  
689 due to climate change. Conversely, negative changes in the ballast effect could potentially

Jorge 4/1/15 6:20 PM

Deleted: expand

Jorge 4/3/15 2:45 PM

Deleted: Moreover

Jorge 4/3/15 2:45 PM

Deleted: Finally, the accurate representation of subsurface O<sub>2</sub> concentration remains as a major challenge for ocean biogeochemical models, as shown by Bopp et al. (2013).

696 reinforce nitrification at shallow depth in response to less efficient POC export to depth  
697 and shallow remineralization (Gehlen et al., 2011). Regarding N<sub>2</sub>O formation via  
698 denitrification, changes in seawater pH as a consequence of higher levels of CO<sub>2</sub> might  
699 not be substantial enough to change the N<sub>2</sub>O production efficiency, assuming a similar  
700 response of marine denitrifiers as reported for denitrifying bacteria have in terrestrial  
701 systems (Liu et al., 2010). Finally, the C:N ratio in export production (Riebesell et al.,  
702 2007) might increase in response to ocean acidification, potentially leading to a greater  
703 expansion of OMZs than simulated here (Oschlies et al., 2008; Tagliabue et al., 2011),  
704 and therefore to enhanced N<sub>2</sub>O production associated with the low-O<sub>2</sub> pathway.  
705 Changes in atmospheric nitrogen deposition have not been considered in this study. It  
706 has been suggested that due to anthropogenic activities the additional amount of reactive  
707 nitrogen in the ocean could fuel primary productivity and N<sub>2</sub>O production. Estimates are  
708 however low, around 3-4% of the total oceanic emissions (Suntharalingam et al., 2012).  
709 Longer simulation periods could reveal additional effects on N<sub>2</sub>O transport beyond  
710 changes in upwelling or meridional transport of N<sub>2</sub>O in the subsurface (Suntharalingam  
711 and Sarmiento, 2000) that have been observed in this transient simulation. Long-term  
712 responses might include eventual ventilation of the N<sub>2</sub>O reservoir in the Southern Ocean,  
713 highlighting the role of upwelling regions as an important source of N<sub>2</sub>O when longer  
714 time periods are considered in model projections. Additional studies using other ocean  
715 biogeochemical models might also yield alternative values using the same  
716 parameterizations. N<sub>2</sub>O production is particularly sensitive to the distribution and  
717 magnitude of export of organic matter and O<sub>2</sub> fields defined in models.

718

## 719 6. Contribution of future N<sub>2</sub>O to climate feedbacks

720

721 Changes in the oceanic emissions of N<sub>2</sub>O to the atmosphere will have an impact on  
722 atmospheric radiative forcing, with potential feedbacks on the climate system. Based on  
723 the estimated 4 to 12% decrease in N<sub>2</sub>O sea-to-air flux over the 21<sup>st</sup> century under  
724 RCP8.5, we estimated the feedback factor for these changes as defined by Xu-Ri et al.  
725 (2012). Considering the reference value of the pre-industrial atmospheric N<sub>2</sub>O  
726 concentration of 280 ppb in equilibrium, and its associated global N<sub>2</sub>O emissions of 11.8  
727 TgN yr<sup>-1</sup>, we quantify the resulting changes in N<sub>2</sub>O concentration per degree for the two

Jorge 3/31/15 3:07 PM

Deleted: close to

Jorge 4/1/15 10:20 AM

Deleted: E

Jorge 4/1/15 10:21 AM

Deleted: at high latitudes could shed light into

732 projected emissions in 2100 using P.TEMP and P.OMZ. The model projects changes in  
733 N<sub>2</sub>O emissions of -0.16 and -0.48 TgN yr<sup>-1</sup> respectively, whereas surface temperature is  
734 assumed to increase globally by 3°C on average according to the physical forcing used in  
735 our simulations. These results yield -0.05 and -0.16 TgN yr<sup>-1</sup> K<sup>-1</sup>, or alternatively -1.25  
736 and -3.80 ppb K<sup>-1</sup> for P.TEMP and P.OMZ respectively. Using Joos et al. (2001) we  
737 calculate the feedback factor in equilibrium for projected changes in emissions to be -  
738 0.005 and -0.014 W m<sup>-2</sup>K<sup>-1</sup> in P.TEMP and P.OMZ.

739 Stocker et al. (2013) projected changes in terrestrial N<sub>2</sub>O emissions in 2100 using  
740 transient model simulations leading to feedback strengths between +0.001 and +0.015 W  
741 m<sup>-2</sup>K<sup>-1</sup>. Feedback strengths associated with the projected decrease of oceanic N<sub>2</sub>O  
742 emissions are of the same order of magnitude as those attributable to changes in the  
743 terrestrial sources of N<sub>2</sub>O, yet opposite in sign, suggesting a compensation of changes in  
744 radiative forcing due to future increasing terrestrial N<sub>2</sub>O emissions. At this stage,  
745 potential compensation between land and ocean emissions is to be taken with caution, as  
746 it relies of a single model run with constant atmospheric N<sub>2</sub>O.

747

## 748 7. Conclusions

749

750 Our simulations suggest that anthropogenic climate change could lead to a global  
751 decrease in oceanic N<sub>2</sub>O emissions during the 21<sup>st</sup> century. This maximum projected  
752 decrease of 12% in marine N<sub>2</sub>O emissions for the business-as-usual high CO<sub>2</sub> emissions  
753 scenario would compensate for the estimated increase in N<sub>2</sub>O fluxes from the terrestrial  
754 biosphere in response to anthropogenic climate change (Stocker et al. 2013), so that the  
755 climate-N<sub>2</sub>O feedback may be more or less neutral over the coming decades.

756 The main mechanisms contributing to the reduction of marine N<sub>2</sub>O emissions are a  
757 decrease in N<sub>2</sub>O production in high oxygenated waters as well as an increase in ocean  
758 vertical stratification that acts to decrease the transport of N<sub>2</sub>O from the sub-surface to  
759 the surface ocean. Despite the decrease in both N<sub>2</sub>O production and N<sub>2</sub>O emissions,  
760 simulations suggest that the global marine N<sub>2</sub>O inventory may increase from 2005 to  
761 2100. This increase is explained by the reduced transport of N<sub>2</sub>O from the production  
762 zones to the air-sea interface.

763 | Differences between the two parameterizations used here are [more related to](#)

764 biogeochemistry rather than changes in ocean circulation. Despite sharing the high-O<sub>2</sub>  
765 N<sub>2</sub>O production pathway, leading to a decrease in N<sub>2</sub>O emissions in both cases, the role  
766 of warming in P.TEMP or higher N<sub>2</sub>O yields at low-O<sub>2</sub> concentrations in P.OMZ,  
767 translate into notable differences in the evolution of the two production pathways.  
768 However, the dominant effect of changes in stratification in both parameterizations  
769 drives ultimately the homogeneous response of the parameterizations considered in  
770 model projections in the next century.  
771 The N<sub>2</sub>O production pathways demand however a better understanding in order to  
772 enable an improved representation of processes in models. At a first order, the efficiencies  
773 of the production processes in response to higher temperatures or increased seawater  
774 pCO<sub>2</sub> are required. Second order effects such as changes in the O<sub>2</sub> boundaries at which  
775 nitrification and denitrification occur must be also taken into account. In the absence of  
776 process-based parameterizations, N<sub>2</sub>O production parameterizations will still rely on  
777 export of organic carbon and oxygen levels. Both need to be improved in global  
778 biogeochemical models.  
779 The same combination of mechanisms (i.e., change in export production and ocean  
780 stratification) have been identified as drivers of changes in oceanic N<sub>2</sub>O emissions during  
781 the Younger Dryas by Goldstein et al. (2003). The N<sub>2</sub>O flux decreased, while the N<sub>2</sub>O  
782 reservoir was fueled by longer residence times of N<sub>2</sub>O caused by increased stratification.  
783 Other studies point towards changes in the N<sub>2</sub>O production at the OMZs as the main  
784 reason for variations in N<sub>2</sub>O observed in the past (Suthhof et al., 2001). Whether these  
785 mechanisms are plausible drivers of changes beyond year 2100 remains an open question  
786 that needs to be addressed with longer simulations.  
787

Jorge 3/31/15 3:27 PM  
Deleted: modest, and

Jorge 3/31/15 3:27 PM  
Deleted: does not

Jorge 3/31/15 3:27 PM  
Deleted: significant

Jorge 3/31/15 3:28 PM  
Deleted: in our model projections.

Jorge 3/31/15 3:29 PM  
Deleted: The dominant high-O<sub>2</sub> N<sub>2</sub>O production pathway drives not only the general decrease in N<sub>2</sub>O emissions but also the homogeneity between the two parameterizations considered.

Jorge 3/31/15 2:45 PM  
Deleted: f

798 8. Acknowledgements

799

800 We thank Cynthia Nevison for providing us the N<sub>2</sub>O sea-to-air flux dataset. We thank  
801 Annette Kock and Herman Bange for the availability of the MEMENTO database  
802 (<https://memento.geomar.de>). We thank Christian Ethé for help analyzing PISCES  
803 model drift. Comments by Parvatha Suntharalingam and three anonymous reviewers  
804 improved significantly this manuscript. Nicolas Gruber acknowledges the support of  
805 ETH Zürich. This work has been supported by the European Union via the Greencycles  
806 II FP7-PEOPLE-ITN-2008, number 238366.



807 7. References

808

- 809 Aumont, O., and Bopp, L.: Globalizing results from ocean in situ iron fertilization studies,  
810 Global Biogeochemical Cycles, [GB2017](#), 20, 10.1029/2005gb002591, 2006.
- 811 Bange, H. W., Rixen, T., Johansen, A. M., Siefert, R. L., Ramesh, R., Ittekkot, V., Hoffmann,  
812 M. R., and Andreae, M. O.: A revised nitrogen budget for the Arabian Sea, Global  
813 Biogeochemical Cycles, 14, 1283-1297, 10.1029/1999gb001228, 2000.
- 814 Bange, H. W., Bell, T. G., Cornejo, M., Freing, A., Uher, G., Upstill-Goddard, R. C., and  
815 Zhang, G.: MEMENTO: a proposal to develop a database of marine nitrous oxide and methane  
816 measurements, Environmental Chemistry, 6, 195-197, 10.1071/en09033, 2009.
- 817 Beman, J. M., Chow, C.-E., King, A. L., Feng, Y., Fuhrman, J. A., Andersson, A., Bates, N. R.,  
818 Popp, B. N., and Hutchins, D. A.: Global declines in oceanic nitrification rates as a consequence  
819 of ocean acidification, Proceedings of the National Academy of Sciences of the United States of  
820 America, 108, 208-213, 10.1073/pnas.1011053108, 2011.
- 821 Bianchi, D., Dunne, J. P., Sarmiento, J. L., and Galbraith, E. D.: Data-based estimates of  
822 suboxia, denitrification, and N<sub>2</sub>O production in the ocean and their sensitivities to dissolved O-  
823 2, Global Biogeochemical Cycles, 26, [GB2009](#), 10.1029/2011gb004209, 2012.
- 824 Bindoff, N., Willebrand, J., Artale, V., Cazenave, A., Gregory, J., Gulev, S., Hanawa, K.,  
825 Le Quere, C., Levitus, S., Norjiri, Y., Shum, C., Talley, L., and Unnikrishnan, A.:  
826 Observations: Oceanic Climate Change and Sea Level, In Climate Change 2007: The  
827 Physical Science Basis. Contribution of Working Group I to the Fourth Assessment  
828 Report of the Intergovernmental Panel on Climate Change, 2007.
- 829 Bopp, L., Resplandy, L., Orr, J. C., Doney, S. C., Dunne, J. P., Gehlen, M., Halloran, P.,  
830 Heinze, C., Ilyina, T., Seferian, R., Tjiputra, J., and Vichi, M.: Multiple stressors of ocean  
831 ecosystems in the 21st century: projections with CMIP5 models, Biogeosciences, 10, 6225-6245,  
832 10.5194/bg-10-6225-2013, 2013.
- 833 Butler, J. H., Elkins, J. W., Thompson, T. M., and Egan, K. B.: Tropospheric and dissolved  
834 N<sub>2</sub>O of the west pacific and east-indian oceans during the el-nino southern oscillation event of  
835 1987, Journal of Geophysical Research-Atmospheres, 94, 14865-14877,  
836 10.1029/JD094iD12p14865, 1989.
- 837 Ciais, P., Sabine, C., Bala, G., Bopp, L., Brovkin, V., Canadell, J., Chhabra, A., DeFries,  
838 R., Galloway, J., Heimann, M., Jones, C., Le Quéré, C., Myneni, RB., Piao, S. and

839 Thornton, P.: Carbon and Other Biogeochemical Cycles. In: Climate Change 2013: The  
840 Physical Science Basis. Contribution of Working Group I to the Fifth Assessment Report  
841 of the Intergovernmental Panel on Climate Change, 2013.

842 Cocco, V., Joos, F., Steinacher, M., Froelicher, T. L., Bopp, L., Dunne, J., Gehlen, M., Heinze,  
843 C., Orr, J., Oschlies, A., Schneider, B., Segschneider, J., and Tjiputra, J.: Oxygen and indicators  
844 of stress for marine life in multi-model global warming projections, *Biogeosciences*, 10, 1849-  
845 1868, 10.5194/bg-10-1849-2013, 2013.

846 Cohen, Y., and Gordon, L. I.: Nitrous-oxide in oxygen minimum of eastern tropical north  
847 pacific - evidence for its consumption during denitrification and possible mechanisms for its  
848 production, *Deep-Sea Research*, 25, 509-524, 10.1016/0146-6291(78)90640-9, 1978.

849 Cohen, Y., and Gordon, L. I.: Nitrous-oxide production in the ocean, *Journal of Geophysical*  
850 *Research-Oceans and Atmospheres*, 84, 347-353, 10.1029/JC084iC01p00347, 1979.

851 Crutzen, P. J.: Influence of nitrogen oxides on atmospheric ozone content, *Quarterly Journal of*  
852 *the Royal Meteorological Society*, 96, 320-326, 10.1002/qj.49709640815, 1970.

853 de Wilde, H. P. J., and de Bie, M. J. M.: Nitrous oxide in the Schelde estuary: production by  
854 nitrification and emission to the atmosphere, *Marine Chemistry*, 69, 203-216, 10.1016/s0304-  
855 4203(99)00106-1, 2000.

856 Deutsch, C., Brix, H., Ito, T., Frenzel, H., and Thompson, L.: Climate-Forced Variability of  
857 Ocean Hypoxia, *Science*, 333, 336-339, 10.1126/science.1202422, 2011.

858 Dufresne, J. L., Foujols, M. A., Denvil, S., Caubel, A., Marti, O., Aumont, O., Balkanski, Y.,  
859 Bekki, S., Bellenger, H., Benshila, R., Bony, S., Bopp, L., Braconnot, P., Brockmann, P.,  
860 Cadule, P., Cheruy, F., Codron, F., Cozic, A., Cugnet, D., de Noblet, N., Duvel, J. P., Ethe, C.,  
861 Fairhead, L., Fichefet, T., Flavoni, S., Friedlingstein, P., Grandpeix, J. Y., Guez, L., Guilyardi,  
862 E., Hauglustaine, D., Hourdin, F., Idelkadi, A., Ghattas, J., Joussaume, S., Kageyama, M.,  
863 Krinner, G., Labetoulle, S., Lahellec, A., Lefebvre, M. P., Lefevre, F., Levy, C., Li, Z. X., Lloyd,  
864 J., Lott, F., Madec, G., Mancip, M., Marchand, M., Masson, S., Meurdesoif, Y., Mignot, J.,  
865 Musat, I., Parouty, S., Polcher, J., Rio, C., Schulz, M., Swingedouw, D., Szopa, S., Talandier,  
866 C., Terray, P., Viovy, N., and Vuichard, N.: Climate change projections using the IPSL-CM5  
867 Earth System Model: from CMIP3 to CMIP5, *Climate Dynamics*, 40, 2123-2165,  
868 10.1007/s00382-012-1636-1, 2013.

869 [Dunne, J. P., Sarmiento, J. L., and Gnanadesikan, A.: A synthesis of global particle export](#)  
870 [from the surface ocean and cycling through the ocean interior and on the seafloor, \*Global\*](#)

Jorge 3/31/15 2:50 PM

Deleted: &

872 | [Biogeochemical Cycles](#), 21, GB4006,10.1029/2006gb002907, 2007.

873 | Elkins, J. W., Wofsy, S. C., McElroy, M. B., Kolb, C. E., and Kaplan, W. A.: Aquatic sources  
874 | and sinks for nitrous-oxide, *Nature*, 275, 602-606, 10.1038/275602a0, 1978.

875 | Farias, L., Paulmier, A., and Gallegos, M.: Nitrous oxide and N-nutrient cycling in the  
876 | oxygen minimum zone off northern Chile, *Deep-Sea Research Part I-Oceanographic*  
877 | *Research Papers*, 54, 164-180, 10.1016/j.dsr.2006.11.003, 2007.

878 | Fletcher, S. E. M., Gruber, N., Jacobson, A. R., Gloor, M., Doney, S. C., Dutkiewicz, S.,  
879 | Gerber, M., Follows, M., Joos, F., Lindsay, K., Menemenlis, D., Mouchet, A., Muller, S. A.,  
880 | and Sarmiento, J. L.: Inverse estimates of the oceanic sources and sinks of natural CO<sub>2</sub> and  
881 | the implied oceanic carbon transport, *Global Biogeochemical Cycles*, 21, GB1010,  
882 | 10.1029/2006gb002751, 2007.

883 | Frame, C. H., and Casciotti, K. L.: Biogeochemical controls and isotopic signatures of nitrous  
884 | oxide production by a marine ammonia-oxidizing bacterium, *Biogeosciences*, 7, 2695-2709,  
885 | 10.5194/bg-7-2695-2010, 2010.

886 | Freing, A., Wallace, D. W. R., Tanhua, T., Walter, S., and Bange, H. W.: North Atlantic  
887 | production of nitrous oxide in the context of changing atmospheric levels, *Global*  
888 | *Biogeochemical Cycles*, 23, GB4015, 10.1029/2009gb003472, 2009.

889 | Freing, A., Wallace, D. W. R., and Bange, H. W.: Global oceanic production of nitrous oxide,  
890 | *Philosophical Transactions of the Royal Society B-Biological Sciences*, 367, 1245-1255,  
891 | 10.1098/rstb.2011.0360, 2012.

892 | Gehlen, M., Gruber, N., Gangstø, R., Bopp, L., and Oschlies, A.: Biogeochemical consequences  
893 | of ocean acidification and feedbacks to the earth system. *Ocean acidification: 230-248*, 2011.

894 | Goldstein, B., Joos, F., and Stocker, T. F.: A modeling study of oceanic nitrous oxide during the  
895 | Younger Dryas cold period, *Geophysical Research Letters*, 30, 1092, 10.1029/2002gl016418,  
896 | 2003.

897 | Goreau, T. J., Kaplan, W. A., Wofsy, S. C., McElroy, M. B., Valois, F. W., and Watson, S. W.:  
898 | Production of NO<sub>2</sub><sup>-</sup> and N<sub>2</sub>O by nitrifying bacteria at reduced concentrations of oxygen, *Applied*  
899 | *and Environmental Microbiology*, 40, 526-532, 1980.

900 | Gruber, N., and Galloway, J. N.: An Earth-system perspective of the global nitrogen cycle,  
901 | *Nature*, 451, 293-296, 10.1038/nature06592, 2008.

902 | Gruber, N.: Warming up, turning sour, losing breath: ocean biogeochemistry under global  
903 | change, *Philosophical Transactions of the Royal Society a-Mathematical Physical and*  
904 | *Engineering Sciences*, 369, 1980-1996, 10.1098/rsta.2011.0003, 2011.

905 Gruber, N.: The marine nitrogen cycle: Overview of distributions and processes. In:  
906 Nitrogen in the marine environment, 2nd edition, 1-50, 2008.

907 Huesemann, M. H., Skillman, A. D., and Crecelius, E. A.: The inhibition of marine nitrification  
908 by ocean disposal of carbon dioxide, *Marine Pollution Bulletin*, 44, 142-148, 10.1016/s0025-  
909 326x(01)00194-1, 2002.

910 Jin, X., and Gruber, N.: Offsetting the radiative benefit of ocean iron fertilization by enhancing  
911 N<sub>2</sub>O emissions, *Geophysical Research Letters*, 30, 2249, 10.1029/2003gl018458, 2003.

912 Johnston, H.: Reduction of stratospheric ozone by nitrogen oxide catalysts from supersonic  
913 transport exhaust, *Science*, 173, 517-522, 10.1126/science.173.3996.517, 1971.

914 Joos, F., Prentice, I. C., Sitch, S., Meyer, R., Hooss, G., Plattner, G. K., Gerber, S., and  
915 Hasselmann, K.: Global warming feedbacks on terrestrial carbon uptake under the  
916 Intergovernmental Panel on Climate Change (IPCC) emission scenarios, *Global Biogeochemical*  
917 *Cycles*, 15, 891-907, 10.1029/2000gb001375, 2001.

918 Keeling, R. F., Koertzing, A., and Gruber, N.: Ocean Deoxygenation in a Warming World,  
919 *Annual Review of Marine Science*, 2, 199-229, 10.1146/annurev.marine.010908.163855, 2010.

920 Liu, B., Morkved, P. T., Frostegard, A., and Bakken, L. R.: Denitrification gene pools,  
921 transcription and kinetics of NO, N<sub>2</sub>O and N-2 production as affected by soil pH, *Fems*  
922 *Microbiology Ecology*, 72, 407-417, 10.1111/j.1574-6941.2010.00856.x, 2010.

923 Mantoura, R. F. C., Law, C. S., Owens, N. J. P., Burkill, P. H., Woodward, E. M. S., Howland,  
924 R. J. M., and Llewellyn, C. A.: Nitrogen biogeochemical cycling in the northwestern indian-  
925 ocean, *Deep-Sea Research Part II-Topical Studies in Oceanography*, 40, 651-671, 1993.

926 Myhre, G., Shindell, D., Bréon, F.-M., Collins, W., Fuglestedt, J., Huang, J., Koch, D.,  
927 Lamarque, J.-F., Lee, D., Mendoza, B., Nakajima, T., Robock, A., Stephens, G.,  
928 Takemura, T. and Zhang, H.: Anthropogenic and Natural Radiative Forcing. In:  
929 *Climate Change 2013: The Physical Science Basis. Contribution of Working Group I to*  
930 *the Fifth Assessment Report of the Intergovernmental Panel on Climate Change*, 2013.

931 Nevison, C. D., Lueker, T. J., and Weiss, R. F.: Quantifying the nitrous oxide source  
932 from coastal upwelling, *Global Biogeochemical Cycles*, 18, GB1018,  
933 10.1029/2003gb002110, 2004.

934 Nevison, C., Butler, J. H., and Elkins, J. W.: Global distribution of N<sub>2</sub>O and the Delta N<sub>2</sub>O-  
935 AOU yield in the subsurface ocean, *Global Biogeochemical Cycles*, 17, 1119,  
936 10.1029/2003gb002068, 2003.

Jorge 3/31/15 2:52 PM

Deleted: &

938 Nevison, C. D., Weiss, R. F., and Erickson, D. J.: Global oceanic emissions of nitrous-oxide,  
939 Journal of Geophysical Research-Oceans, 100, 15809-15820, 10.1029/95jc00684, 1995.  
940 Oschlies, A., Schulz, K. G., Riebesell, U., and Schmittner, A.: Simulated 21st century's increase  
941 in oceanic suboxia by CO<sub>2</sub>-enhanced biotic carbon export, Global Biogeochemical Cycles, 22,  
942 [GB4008](#), 10.1029/2007gb003147, 2008.  
943 Prather, M. J., Holmes, C. D., and Hsu, J.: Reactive greenhouse gas scenarios: Systematic  
944 exploration of uncertainties and the role of atmospheric chemistry, Geophysical Research Letters,  
945 39, [L09803](#), 10.1029/2012gl051440, 2012.  
946 Punshon, S., and Moore, R. M.: Nitrous oxide production and consumption in a eutrophic  
947 coastal embayment, Marine Chemistry, 91, 37-51, 10.1016/j.marchem.2004.04.003, 2004.  
948 Ravishankara, A. R., Daniel, J. S., and Portmann, R. W.: Nitrous Oxide (N<sub>2</sub>O): The Dominant  
949 Ozone-Depleting Substance Emitted in the 21st Century, Science, 326, 123-125,  
950 10.1126/science.1176985, 2009.  
951 Resplandy, L., Levy, M., Bopp, L., Echevin, V., Pous, S., Sarma, V. V. S. S., and Kumar, D.:  
952 Controlling factors of the oxygen balance in the Arabian Sea's OMZ, Biogeosciences, 9, 5095-  
953 5109, 10.5194/bg-9-5095-2012, 2012.  
954 Riebesell, U., Schulz, K. G., Bellerby, R. G. J., Botros, M., Fritsche, P., Meyerhoefer, M., Neill,  
955 C., Nondal, G., Oschlies, A., Wohlers, J., and Zoellner, E.: Enhanced biological carbon  
956 consumption in a high CO<sub>2</sub> ocean, Nature, 450, 545-548, 10.1038/nature06267, 2007.  
957 Sarmiento, J. L., Slater, R., Barber, R., Bopp, L., Doney, S. C., Hirst, A. C., Kleypas, J., Matear,  
958 R., Mikolajewicz, U., Monfray, P., Soldatov, V., Spall, S. A., and Stouffer, R.: Response of ocean  
959 ecosystems to climate warming, Global Biogeochemical Cycles, 18, [GB3003](#),  
960 10.1029/2003gb002134, 2004.  
961 Steinacher, M., Joos, F., Frolicher, T. L., Bopp, L., Cadule, P., Cocco, V., Doney, S. C., Gehlen,  
962 M., Lindsay, K., Moore, J. K., Schneider, B., and Segschneider, J.: Projected 21st century  
963 decrease in marine productivity: a multi-model analysis, Biogeosciences, 7, 979-1005, 2010.  
964 Stocker, B. D., Roth, R., Joos, F., Spahni, R., Steinacher, M., Zaehle, S., Bouwman, L., Xu, R.,  
965 and Prentice, I. C.: Multiple greenhouse-gas feedbacks from the land biosphere under future  
966 climate change scenarios, Nature Climate Change, 3, 666-672, 10.1038/nclimate1864, 2013.  
967 Suntharalingam, P., and Sarmiento, J. L.: Factors governing the oceanic nitrous oxide  
968 distribution: Simulations with an ocean general circulation model, Global Biogeochemical  
969 Cycles, 14, 429-454, 10.1029/1999gb900032, 2000.

Jorge 3/31/15 2:54 PM

Deleted: U510

971 Suntharalingam, P., Sarmiento, J. L., and Toggweiler, J. R.: Global significance of nitrous-oxide  
972 production and transport from oceanic low-oxygen zones: A modeling study, *Global*  
973 *Biogeochemical Cycles*, 14, 1353-1370, 10.1029/1999gb900100, 2000.

974 Suntharalingam, P., Buitenhuis, E., Le Quere, C., Dentener, F., Nevison, C., Butler, J. H.,  
975 Bange, H. W., and Forster, G.: Quantifying the impact of anthropogenic nitrogen deposition on  
976 oceanic nitrous oxide, *Geophysical Research Letters*, 39, L07605, 10.1029/2011gl050778, 2012.

977 [Suthhof, A., Ittekkot, V., and Gaye-Haake, B.: Millennial-scale oscillation of denitrification](#)  
978 [intensity in the Arabian Sea during the late Quaternary and its potential influence on](#)  
979 [atmospheric N<sub>2</sub>O and global climate, \*Global Biogeochemical Cycles\*, 15, 637-649,](#)  
980 [10.1029/2000gb001337, 2001.](#)

981 Tagliabue, A., Bopp, L., and Gehlen, M.: The response of marine carbon and nutrient cycles to  
982 ocean acidification: Large uncertainties related to phytoplankton physiological assumptions,  
983 *Global Biogeochemical Cycles*, 25, GB3017, 10.1029/2010gb003929, 2011.

984 Takahashi, T., Broecker, W. S., and Langer, S.: Redfield ratio based on chemical-data from  
985 isopycnal surfaces, *Journal of Geophysical Research-Oceans*, 90, 6907-6924,  
986 10.1029/JC090iC04p06907, 1985.

987 Tiedje, J.M.: Ecology of denitrification and dissimilatory nitrate reduction to  
988 ammonium. *Biology of anaerobic microorganisms*, 179-244, 1988.

989 Wanninkhof, R.: Relationship between wind-speed and gas-exchange over the ocean, *Journal of*  
990 *Geophysical Research-Oceans*, 97, 7373-7382, 10.1029/92jc00188, 1992.

991 Weiss, R. F., and Price, B. A.: Nitrous-oxide solubility in water and seawater, *Marine Chemistry*,  
992 8, 347-359, 10.1016/0304-4203(80)90024-9, 1980.

993 [Westley, M. B., Yamagishi, H., Popp, B. N., and Yoshida, N.: Nitrous oxide cycling in the](#)  
994 [Black Sea inferred from stable isotope and isotopomer distributions, \*Deep-Sea Research Part\*](#)  
995 [II-Topical Studies in Oceanography](#), 53, 1802-1816, 10.1016/j.dsr2.2006.03.012, 2006.

996 Yoshida, N., Morimoto, H., Hirano, M., Koike, I., Matsuo, S., Wada, E., Saino, T., and  
997 Hattori, A.: Nitrification rates and N-15 abundances of N<sub>2</sub>O and NO<sub>3</sub><sup>-</sup> in the western north  
998 pacific, *Nature*, 342, 895-897, 10.1038/342895a0, 1989.

999 [Zamora, L. M., and Oschlies, A.: Surface nitrification: A major uncertainty in marine N<sub>2</sub>O](#)  
1000 [emissions, \*Geophysical Research Letters\*, 41, 4247-4253, 10.1002/2014gl060556, 2014.](#)

1001 Zamora, L. M., Oschlies, A., Bange, H. W., Huebert, K. B., Craig, J. D., Kock, A., and  
1002 Loescher, C. R.: Nitrous oxide dynamics in low oxygen regions of the Pacific: insights from the  
1003 MEMENTO database, *Biogeosciences*, 9, 5007-5022, 10.5194/bg-9-5007-2012, 2012.

1004 Zehr, J. P., and Ward, B. B.: Nitrogen cycling in the ocean: New perspectives on processes and  
1005 paradigms, *Applied and Environmental Microbiology*, 68, 1015-1024, 10.1128/aem.68.3.1015-  
1006 1024.2002, 2002.  
1007

1008 Table 1: Standard deviation and correlation coefficients between P.TEMP and P.OMZ  
1009 parameterizations with respect to MEMENTO database observations (Bange et al., 2009).  
1010

	P.TEMP	P.OMZ	OBS
Standard deviation (in nmol N <sub>2</sub> O L <sup>-1</sup> )	12	18	16
Correlation coefficient with obs.	0.49	0.42	-

1011  
1012



Table S1: Box model boundary conditions and parameters. NEMO-PISCES model output values are taken from the historical averaged 1985 to 2005 time period and the future averaged 2080 to 2100 time period.

parameter	quantity	units	source
surface N <sub>2</sub> O	10	TgN	PISCES model output
deep N <sub>2</sub> O	1000	TgN	PISCES model output
yield N <sub>2</sub> O produced from POC (ε)	0.0025	mol N <sub>2</sub> O / mol C	Nevison et al. (2003)
ratio of surface N <sub>2</sub> O outgassed (γ)	0.8	mol N <sub>2</sub> O air / mol N <sub>2</sub> O surface	assumption that most of the surface N <sub>2</sub> O is outgassed.
ratio of surface N <sub>2</sub> O exchanged with the deep N <sub>2</sub> O compartment (ν)	0.4	mol N <sub>2</sub> O surface / mol N <sub>2</sub> O deep	box model assumption
export POC @100m in 2005	6.22	PgC yr <sup>-1</sup>	PISCES model output
export POC @100m in 2100	5.30	PgC yr <sup>-1</sup>	PISCES model output

1013

1014

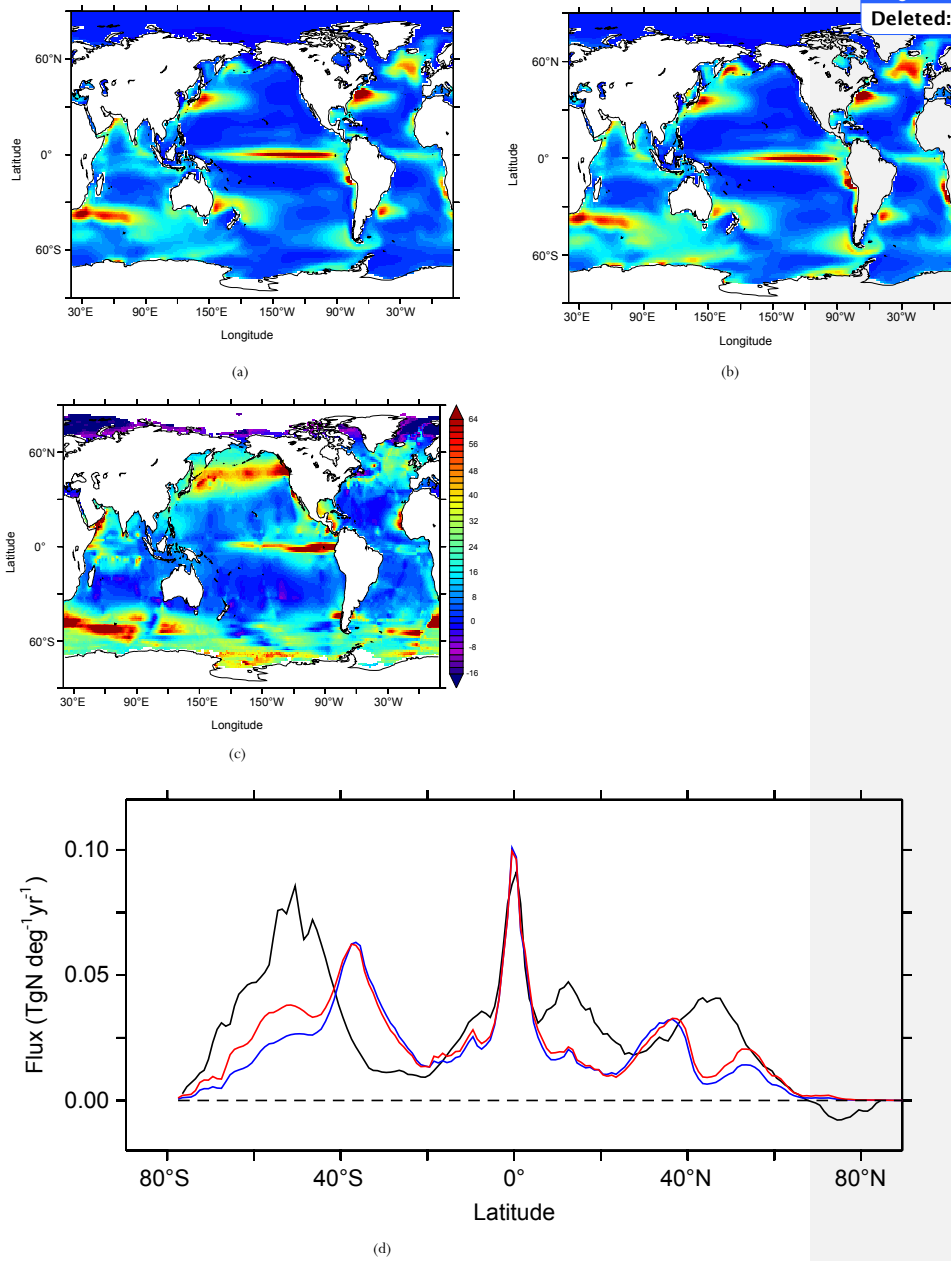
Jorge 3/31/15 3:13 PM  
Deleted: yield sea-to-air

Jorge 3/31/15 3:13 PM  
Deleted: flux

Jorge 3/31/15 3:12 PM  
Deleted: k

1018 Fig. 1: N<sub>2</sub>O sea-to-air flux (in mgN m<sup>-2</sup> yr<sup>-1</sup>) from (a) P.TEMP parameterization averaged for the  
1019 1985 to 2005 time period in the historical simulation, (b) P.OMZ parameterization over the  
1020 same time period, (c) data product of Nevison et al. (2004) and (d) latitudinal N<sub>2</sub>O sea-to-air  
1021 flux (in TgN deg<sup>-1</sup> yr<sup>-1</sup>) from Nevison et al. (2004) (black), P.TEMP (blue) and P.OMZ (red).

1022  
1023  
1024  
1025  
1026



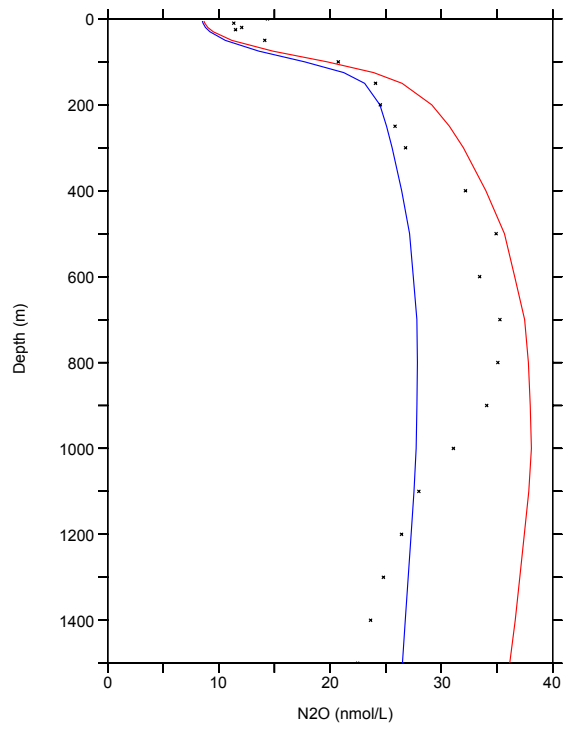
Jorge 4/1/15 2:42 PM

Deleted: 1995

Jorge 4/1/15 2:42 PM

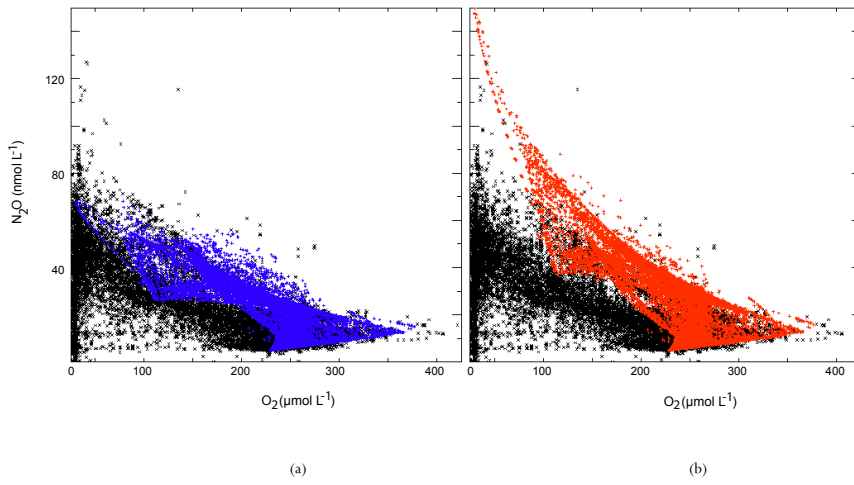
Deleted: 1995

1029 Fig.2: Global average depth profile of N<sub>2</sub>O concentration (in nmol L<sup>-1</sup>) from the MEMENTO  
1030 database (dots) (Bange et al., 2009), P.TEMP (blue) and P.OMZ (red). Model  
1031 parameterizations are averaged over the 1985 to 2005 time period from the historical  
1032 simulation.



1033  
1034

1035 Fig.3: Relationship between O<sub>2</sub> concentration (in μmol L<sup>-1</sup>) and N<sub>2</sub>O concentration (in nmol L<sup>-1</sup>)  
 1036 in the MEMENTO database (black) (Bange et al., 2009), compared to model (a) P.TEMP (blue)  
 1037 and (b) P.OMZ (red) parameterizations averaged over the 1985 to 2005 time period from the  
 1038 historical simulation.

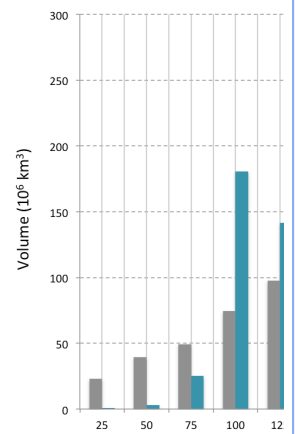


1039  
 1040  
 1041  
 1042  
 1043  
 1044

Jorge 4/3/15 2:16 PM

**Deleted:** (c) Distribution of O<sub>2</sub> concentration in NEMO-PISCES 1985 to 2005 averaged time period (blue) compared to the oxygen corrected World Ocean Atlas (grey) from Bianchi et al. (2012).

Jorge 4/1/15 12:22 PM

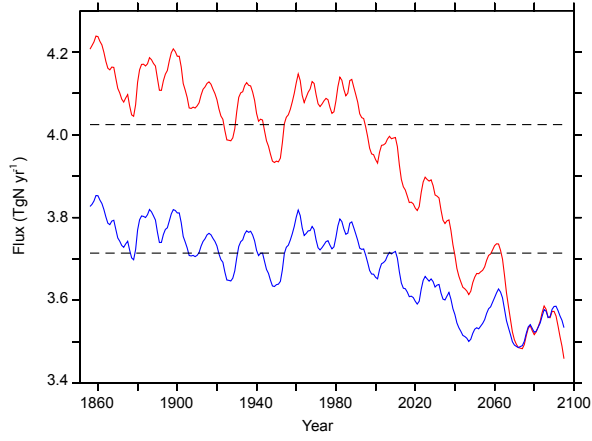


**Deleted:**

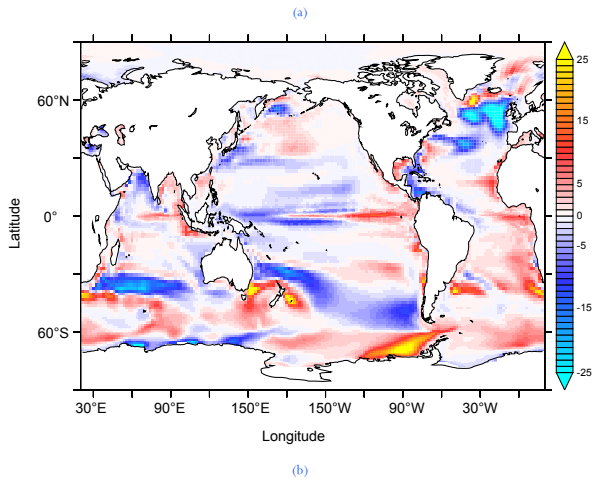
Jorge 4/3/15 2:18 PM

**Deleted:** (c)

1051 Fig 4: (a)  $\text{N}_2\text{O}$  sea-to-air flux (in  $\text{TgN yr}^{-1}$ ) from 1851 to 2100 in P.TEMP (blue) and P.OMZ  
1052 (red) using the historical and future RCP8.5 simulations. Dashed lines indicate the mean value  
1053 over the 1985 to 2005 time period. Change in  $\text{N}_2\text{O}$  sea-to-air flux ( $\text{mgN m}^{-2}\text{yr}^{-1}$ ) from the  
1054 averaged 2080-2100 to 1985-2005 time periods in future RCP8.5 and historical simulations in  
1055 (b) P.TEMP and (c) P.OMZ parameterizations.



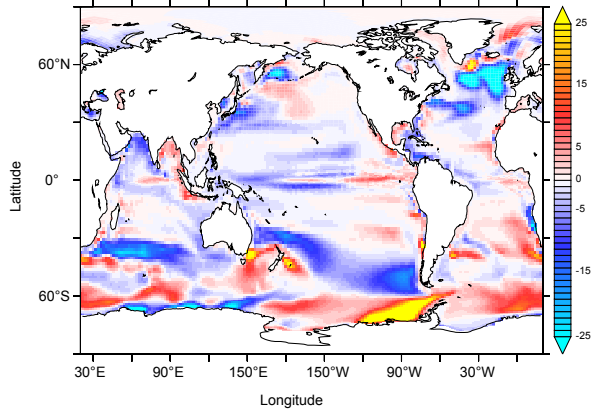
1056  
1057



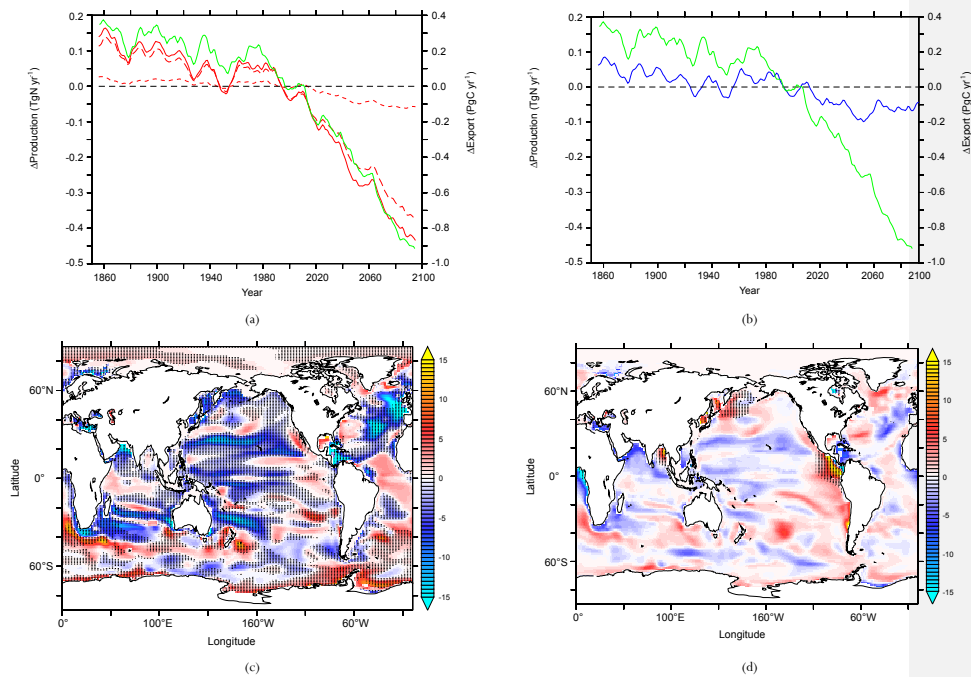
1058  
1059  
1060

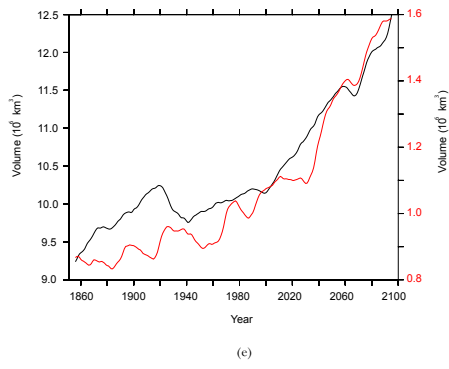
1061  
1062

(c)



1063 Fig 5: (a) Anomalies in export of organic matter at 100m (green), low-O<sub>2</sub> production pathway  
 1064 (short dashed red), high-O<sub>2</sub> production pathway (long dashed red) and total P.OMZ production  
 1065 (red) from 1851 to 2100 using the historical and future RCP8.5 simulations. (b) Anomalies in  
 1066 export of organic matter at 100m (green) and P.TEMP production (blue) over the same time  
 1067 period. (c) Change in high-O<sub>2</sub> production pathway of N<sub>2</sub>O (in mgN m<sup>-2</sup> yr<sup>-1</sup>) in the upper  
 1068 1500m between 2080-2100 to 1985-2005 averaged time periods. Hatched areas indicate  
 1069 regions where change in export of organic matter at 100m deep have the same sign as in  
 1070 changes in high-O<sub>2</sub> production pathway. (d) Change in low-O<sub>2</sub> production pathway of N<sub>2</sub>O (in  
 1071 mgN m<sup>-2</sup> yr<sup>-1</sup>) in the upper 1500m between 2080-2100 to 1985-2005 averaged time periods.  
 1072 Hatched areas indicate regions where oxygen minimum zones (O<sub>2</sub> < 5 μmol L<sup>-1</sup>) expand.  
 1073 Volume (in 10<sup>6</sup> km<sup>3</sup>) of hypoxic (black, O<sub>2</sub> < 60 μmol L<sup>-1</sup>) and suboxic (red, O<sub>2</sub> < 5 μmol L<sup>-1</sup>)  
 1074 areas in the 1851 to 2100 period in NEMO-PISCES historical and future RCP8.5 simulations.  
 1075

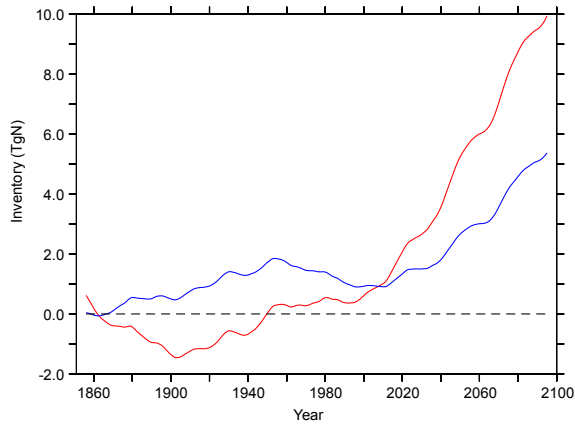




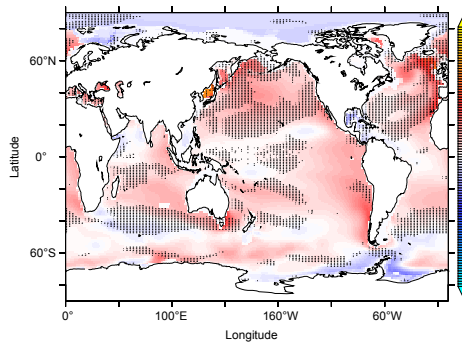
1076  
1077



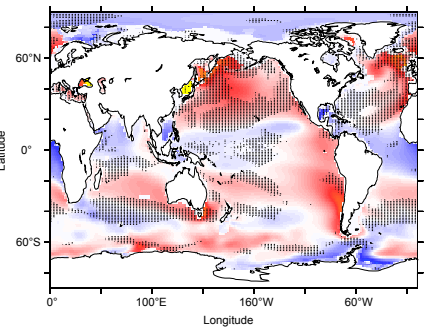
1078 Fig 6: (a) Anomalies in N<sub>2</sub>O inventory (in TgN) from 1851 to 2100 in P.TEMP (blue) and  
1079 P.OMZ (red) using the historical and future RCP8.5 simulations in the upper 1500m. Change  
1080 in vertically integrated N<sub>2</sub>O concentration (in mgN m<sup>-2</sup>) in the upper 1500m using NEMO-  
1081 PISCES model mean from the averaged 2080-2100 to 1985-2005 time periods in future  
1082 RCP8.5 and historical scenarios respectively in (b) P.TEMP and (c) P.OMZ. Hatched areas  
1083 indicate regions where the annual mean mixed layer depth is reduced by more than 5m in  
1084 2080-2100 compared to 1985-2005.



(a)



(b)

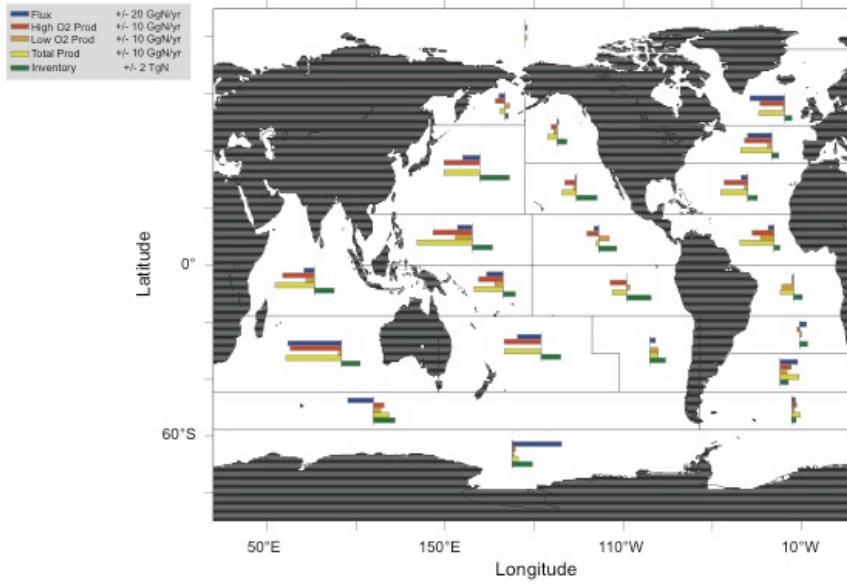


(c)

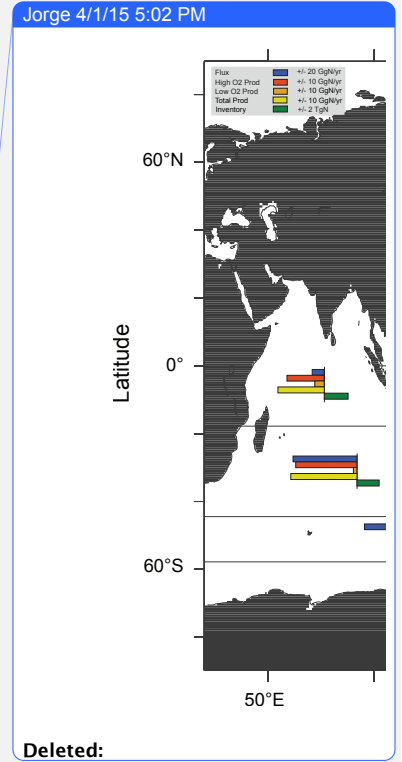
1085  
1086  
1087

1088  
1089

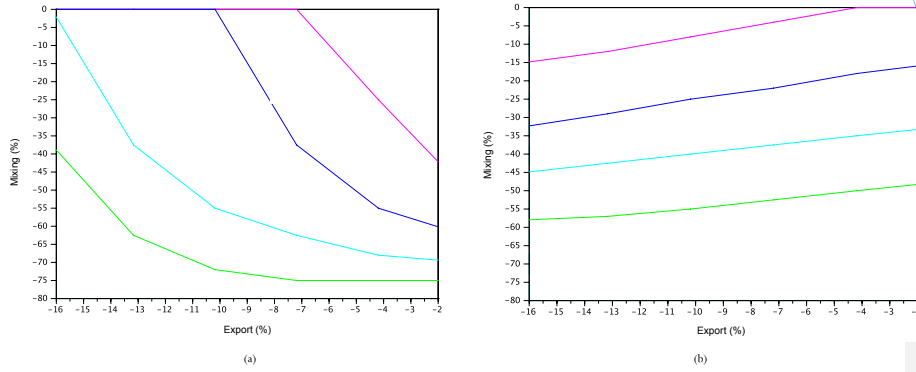
1090 Fig. 7: Change in the whole water column in N<sub>2</sub>O sea-to-air flux (blue), high-O<sub>2</sub> production  
1091 pathway (red), low-O<sub>2</sub> production pathway (orange), total N<sub>2</sub>O production (yellow) and N<sub>2</sub>O  
1092 inventory (green) for P.OMZ from the averaged 2080-2100 to present 1985-2005 averaged  
1093 time period in the NEMO-PISCES historical and future RCP8.5 simulations (based on Mikaloff-  
1094 Fletcher et al. (2006) oceanic regions).



1095  
1096



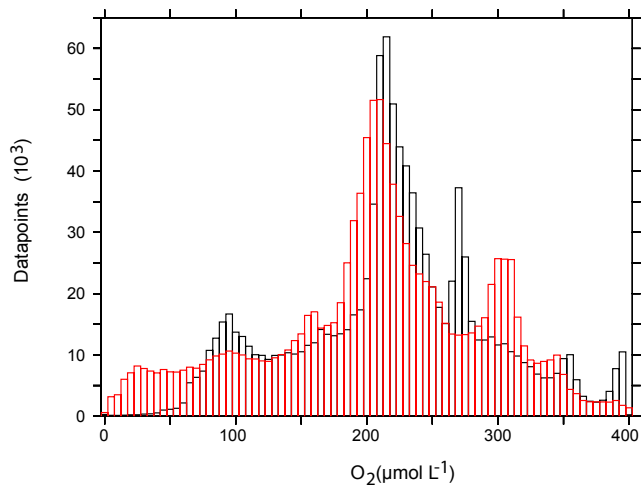
1098 Fig. 8: Box model results, analyzing the effect of changes in ocean circulation by reducing the  
 1099 mixing coefficient ( $\mu$  in %) and changes in biogeochemistry by reducing export of organic  
 1100 matter (in %) separately in  $N_2O$  sea-to-air emissions and  $N_2O$  inventory in 2100. (a) Constant  
 1101 regimes in percentage of the historical  $N_2O$  sea-to-air flux; 95% pink, 90% blue, 85% cyan and  
 1102 80% green, and (b) Constant regimes in percentage of the historical  $N_2O$  concentration in the  
 1103 deep; 90% pink, 110% blue, 125% cyan and 150% green.



1105

- Jorge 3/31/15 3:00 PM  
Deleted: of (a)
- Jorge 3/31/15 3:00 PM  
Deleted: (in percentage of the historical flux)
- Jorge 3/31/15 3:01 PM  
Deleted: )
- Jorge 3/31/15 3:01 PM  
Deleted: (in percentage of the historical concentration)
- Jorge 3/31/15 3:01 PM  
Deleted: ) in 2100 as a result of a reduction in the export coefficient  $e$  (in %) and in the mixing coefficient  $\mu$  (in %) in the box model.

1114 Figure 9: Distribution of O<sub>2</sub> concentration in NEMO-PISCES 1985 to 2005 averaged time  
1115 period (black) compared to the oxygen-corrected World Ocean Atlas (red) from Bianchi et al.  
1116 (2012). Interval widths are O<sub>2</sub> concentrations at steps of 5 μmol L<sup>-1</sup>.

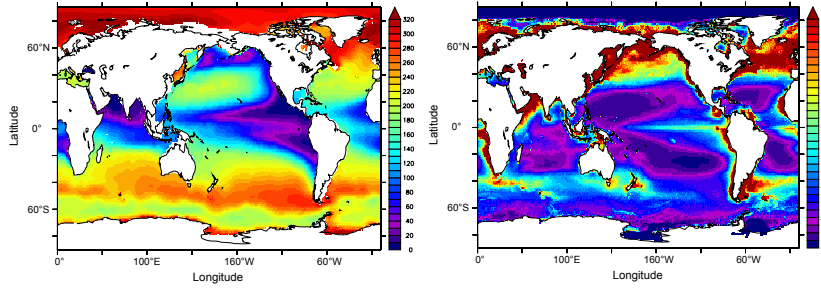


1117

1118

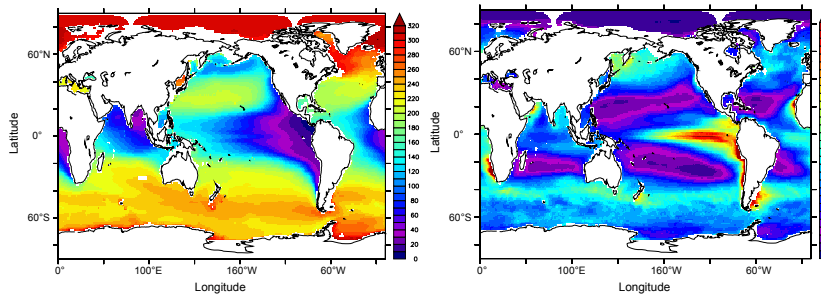
1119 Figure 10: Averaged O<sub>2</sub> concentration between 200-600m depth (in  $\mu\text{mol L}^{-1}$ ) (left) and export  
1120 of carbon (in  $\text{mmolC m}^{-2} \text{d}^{-1}$ ) (right) in (a) WOA2005\* and Dunne et al. (2007), (b) CMIP5  
1121 model mean historical simulations over the 1985-2005 time period and (c) NEMO-PISCES for  
1122 the present 1985-2005 time period.

1123 a. WOA2005\* and Dunne et al., 2007



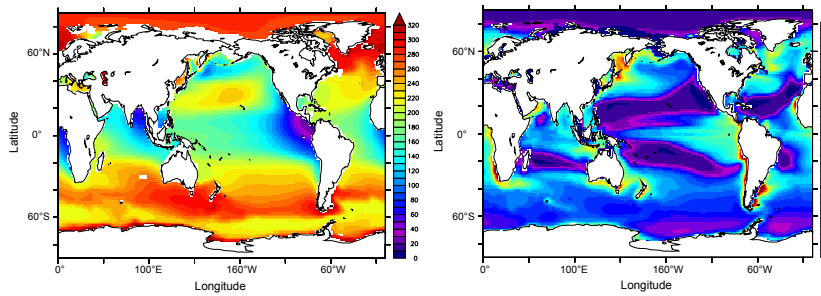
1124

1125 b. CMIP5 model mean



1126

1127 c. NEMO-PISCES



1128

1129 SUPPLEMENTARY MATERIAL

1130

1131 The  $O_2$  modulation function  $f(O_2)$  in P.OMZ is defined as,

$$f(O_2) = \left\{ \begin{array}{ll} \frac{O_2}{O_2^{*1}} & O_2 < O_2^{*1} \\ 1 & O_2^{*1} < O_2 < O_2^{*2} \\ 0.7 \cdot \exp - 0.5(O_2 - O_2^{*2})/O_2^{*2} + \\ 0.3 \cdot \exp - 0.05(O_2 - O_2^{*2})/O_2^{*2} & O_2 \geq O_2^{*2} \end{array} \right\}$$

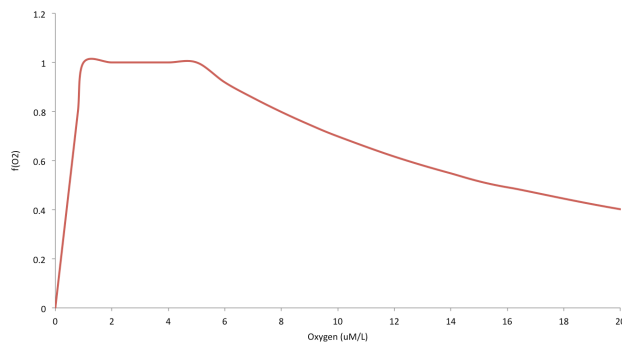
1132

1133 where  $O_2^{*1}$  is  $1 \mu\text{mol L}^{-1}$  and  $O_2^{*2}$  is  $5 \mu\text{mol L}^{-1}$ . The shape of the function is shown in Fig. S1.

1134

1135 Fig. S1: Oxygen modulating function  $f(O_2)$  in the low- $O_2$  production pathway term included in

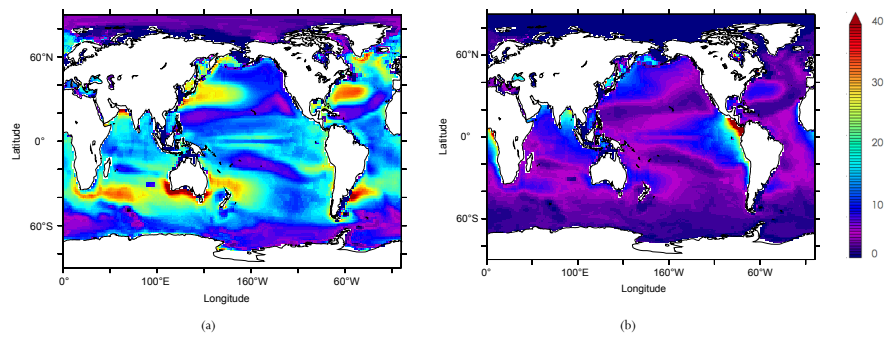
1136 P.OMZ from Goreau et al. (1980).



1137

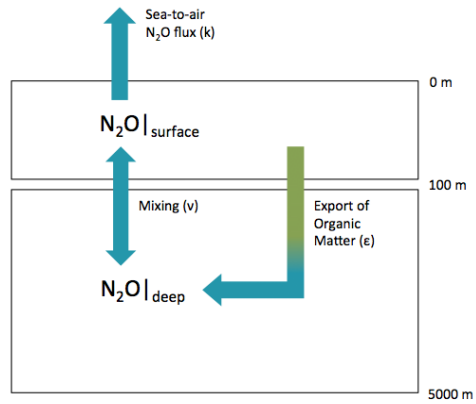
1138

1139 Fig. S2: Vertically integrated (a) high-O<sub>2</sub> and (b) low-O<sub>2</sub> production pathways (in gN m<sup>-2</sup> yr<sup>-1</sup>)  
1140 in P.OMZ for the averaged 1985 to 2005 historical simulation.  
1141



1142  
1143

1144 Fig. S3: Diagram of the box model. N<sub>2</sub>O inventory is separated into surface and deep  
1145 concentrations above and below 100m. The fraction of N<sub>2</sub>O outgassed to the atmosphere ( $k$ ),  
1146 mixing ratio ( $v$ ) between deep and surface and the rate of N<sub>2</sub>O production from the export of  
1147 organic matter to depth ( $e$ ) regulate the N<sub>2</sub>O budget in the ocean interior.



1148  
1149